Louisiana State University

LSU Scholarly Repository

2013

Sedimentation of swarms of particles at low and moderate Reynolds numbers

Oladapo Olanrewaju Ayeni
Louisiana State University and Agricultural and Mechanical College

Follow this and additional works at: https://repository.lsu.edu/gradschool_theses

Part of the Chemical Engineering Commons

Recommended Citation

SEDIMENTATION OF SWARMS OF PARTICLES AT LOW AND MODERATE REYNOLDS NUMBERS

A Thesis

Submitted to the Graduate Faculty of the
Louisiana State University and
Agricultural and Mechanical College
in partial fulfillment of the
requirements for the degree of
Master of Science

in

The Cain Department of Chemical Engineering

by
Oladapo Olanrewaju Ayeni
B.S., University of Lagos, 2006
August 2013

Acknowledgements

I owe a debt of gratitude to my advisor, Professor Krishnaswamy Nandakumar for his guidance throughout this work and for constantly encouraging me to see the big picture and the relevance of the work and pushing me to bring more detail into the analysis and also for providing the resources for this work.

Special mention must be made of Dr. Chunliang Wu whose DPM code formed the basis of this work. I cannot adequately stress how important his support has been not just to this work but to my overall graduate experience

Appreciation must go to Dr. Dandina Rao and Dr. Qin Chen for offering to serve on my committee.

I wish to thank Dr. Rupesh Reddy who first suggested the interesting area of particle swarms, Dr. Mranal Jain, Yuehao Li who gave me a first look at how to organize this document, Tom Scherr, Abhijit Rao and Gongqiang He all of whom have provided a source of invaluable discussions and test bed for the ideas in this work.

I would like to appreciate my parents whose prayers and love I can count on and members of my adopted family here in Baton Rouge at the Bethany World Prayer Center.

The Louisiana Optical Network Initiative and the Louisiana State University High Performance Computing are also acknowledged for the supercomputing clusters used in running the simulations.

"I can do all things through Christ" - Philippians 4:13

Table of Contents

List of Tables

List of Figures

Notation

Symbols
u_s – Settling Velocity of Suspension (m/s)
u_0 – Terminal settling velocity of single particle (m/s)
φ – Solids volume fraction
G, ψ – Arbitrary quantity
$\boldsymbol{x}$ – Position vector (m)
P – Probability distribution
ℭ – Particle configuration
N – Number of particles
ϵ – Ratio of particle radius to cloud radius
R – Radius of cloud (m)
a – Radius of particle (m)
d – Mean particle spacing (m)
Re – Reynolds number
ρ – Density (kg/m^3)
g – Acceleration due to gravity (m/s)
μ – Dynamic viscosity (Pa-s)
St – Stokes number
l – Inertial length (m)
Fr – Froude number
ξ – Correlation length (m)
V – Volume (m^3)
n – Number density of particles
β – Interphase momentum coefficient (N/m^4)
C_D – Drag coefficient
ε – Volume fraction of continuous phase
k – Spring constant
e – Restitution coefficient
ω – Angular velocity (rad/s)
η – Damping coefficient

Subscripts
s – Solids
N – Number of particles
c – Cloud
p – Particle
k – Index
τ – Particle response time
S – Momentum source
m – Mass
n – Normal
t – Tangential
γ – Aspect ratio
b - Breakup

Superscripts
* - Normalized quantity

Abbreviations
DPM – Discrete Particle Model
VACF – Velocity Auto-Correlation Function

Abstract

The sedimentation of a cloud of particles in a viscous fluid at low and moderate Reynolds numbers has been studied using an Eulerian-Lagrangian multiphase flow approach.

We looked at the volume fraction dependence of the settling cloud and find a similar dependence in the simulations as in the theoretical predictions of (Nitsche and Batchelor 1997). The average cloud settling velocity and the velocity fluctuations around this average are found to have a functional dependence on $\varphi^{1/3}$ at negligible Reynolds number. The velocity fluctuations display strong anisotropy with the magnitude of the vertical component almost three times the magnitude of the horizontal component.

Similarities in the interaction between a system of two particle clouds and a system of two immiscible droplets was established with an observed increase in the velocity of the trailing cloud due to drag reduction in the wake of the leading cloud. The formation of the stagnation points at the leading front of the cloud is pointed to as the cause of shape deformation in these systems.

Particle leakage at low Reynolds number was established and found to be directly related to the initial number of particles

At higher Reynolds numbers, the cloud of particles evolved into an open torus and subsequently losing its axi-symmetry and breaking-up into a number of secondary clouds. This process is a type of Rayleigh-Taylor instability and the number of secondary drops was found in our simulations to be dependent on the shape of the boundaries of the flow domain used rather than the nature of the boundaries.

Breakup at moderate Re_c is found to occur after a critical aspect ratio is reached and a scaling

was proposed for dependence of the breakup length and breakup time on Re_c.

1.0   Introduction

When a phase is distributed in another but is not materially connected to it, the system is called dispersion. Dispersions of solid particles suspended in a fluid of lesser density tend to settle out of suspension because of the density difference that exists between the dispersed and the continuous phase in a process called sedimentation. Sedimentation is thus a multi-phase description that differs from multicomponent flow where the constituents are mixed on a microscopic scale.

Sedimentation is an important process employed in many industrial processes and is utilized in processes where the density and size distributions of suspended particles can be exploited for phase separation. Processes such as the clarification of sugar bagasse, water treatment or pre-treatment of metal ores all employ this principle.

Some large-scale natural occurrences that involve sedimentation include the flow of solid and liquid in volcanic eruptions, flow of sediment down a slope in lakes (Pignatel, Nicolas et al. 2011) and the open water disposal of sediments and dredging of coastal waters (Rahimipour and Wilkinson 1992). An understanding of the dynamics of particle dispersion in a liquid solid system can help improve placement of sand and reduce the number of times dredging activities have to be carried out. On a smaller scale, deposits of fat inside arteries (Motomiya and Karino 1984) and flow of blood corpuscles also fall under liquid-solid flows and involve sedimentation.

Other liquid solid systems that require some knowledge of sedimentation include industrial activities such as hydro-transport of particles like coal, or cuttings that result from drilling activities in the oil and gas industry. Also of interest is the transport of micro-sensors to fractures

within rock formations that would report back information about the nature of the formation (Pyrak-Nolte and Olander).

The density imbalance in a liquid-solid mixture ensures that the system continues to evolve until observable segregation takes place e.g. the fluid at the top of the vessel becomes clear and the suspension at the bottom becomes more concentrated. Even though the buoyancy and the drag on the individual particle act at the microscopic scale, they influence interesting large-scale dynamics of the system.

Sedimentation is naturally a "non-equilibrium" phenomenon. Unlike in fluidization where steady state can be described as the point at which the drag exerted on the particles by the inlet fluid stream balances the weight of the bed, thus allowing us to describe a minimum fluidization velocity, we cannot physically describe an equilibrium point in sedimentation except for theoretical investigations where a periodic boundary condition is used in the direction of gravity (Kuusela 2005) or the system is neutrally buoyant thus permitting the equilibrating effect of Brownian fluctuations. The focus of this work would be on particle-liquid systems where the density ratio is substantially greater than one and on inhomogeneous sedimentation where the volume fraction of solids is confined to a finite volume within the clear continuous phase.
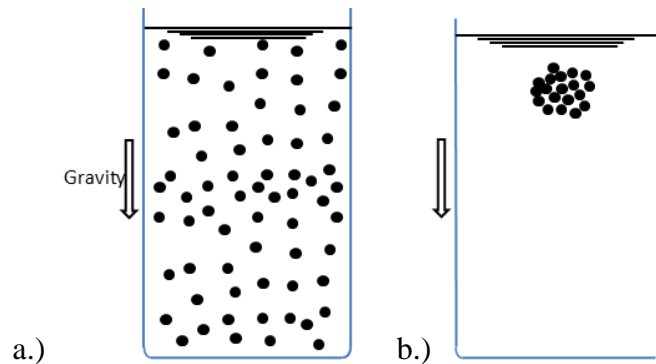
Figure 1.1: Illustration of Homogeneous (left) and inhomogeneous (right) dispersions

The complete description of the inter-particle, hydrodynamic, thermal and external forces acting on a suspension of particles and their spatial distribution is known as the microstructure (Brady and Bossis 1988). The microstructure and the statistics of the suspension evolve with time to become increasingly disorderly. We may simplify the model by legitimately assuming that particles studied in all simulations are large enough for Brownian effect to be neglected and that some form of continuum description of the fluid can be obtained based on the volume fraction of the phases.

The concern in this work is with the fundamental problem of the sedimentation of a cloud of particles in an otherwise clear liquid. The terms cloud, blobs and suspension drops are taken to mean an initially spherical swarm of solid particles in a viscous fluid. As the cloud settles under the influence of gravity, a number of things could occur including particle leakage (Nitsche and Batchelor 1997) and pattern formation due to breakup (Bosse, Kleiser et al. 2005) depending on the flow conditions. Traditionally, the method of simulation has been to use a description that preserves the linearity of the governing equations for the fluid phase e.g. using Stokeslet simulations or Oseenlet simulations which are slight variation of the Stokeslet (Nitsche and Batchelor 1997; Machu, Meile et al. 2001; Metzger, Nicolas et al. 2007; Pignatel, Nicolas et al. 2011). In the model used in this work, the finite volume – lagrangian tracking approach deployed does not neglect the non-linear inertia term in the governing equation.

The aim of this work is to investigate the breakup features of a settling cloud and analyze the effects of inertia, initial volume fraction, nature, size and shape of the boundaries and material properties on the shape instabilities of the blob. Some of these effects have been studied in the context of homogenous sedimentation and at low Reynolds numbers. The significance of isolating the behavior of a cloud is in the broader picture of analyzing the effect of cluster

3

formation and persistence on the dynamics of homogenous sedimentation and multiphase systems in general where one phase is dispersed in another. Mixing and Segregation are issues that are also directly impacted by the behavior of particle blobs.

A summary of some of the various studies that have been performed regarding both homogeneous and inhomogeneous sedimentation are presented in chapter 2. In chapter 3 we present the governing equations used in the simulations and physical justification for the approach used. The statistical tools for analyzing the evolution of particle clouds are introduced. Chapter 4 focuses on the validation of the simulations against data from experiments and theoretical formulations as presented in the literature and analysis of the results. We conclude in Chapter 5 by drawing conclusions from the results of the simulations.

2.0   Literature Review

In contrast to gas-solid system where inter-particle collisions are frequent and the solid phase can be modeled as an ideal gas using the kinetic theory for granular flow (Gidaspow 1994), the dynamics of liquid solid systems is dominated by long-range hydrodynamic interactions. If the particle diameter is >10μm, the effect of thermal fluctuations in the fluid phase can be neglected in deference to the hydrodynamic interactions (Nguyen and Ladd 2005). Research into liquid solid systems is not new and the focus has ranged from instabilities in the structural patterns of settling swarms of particles to the influence of boundaries on the fluctuation of particle velocities around a mean value.

A number of methods have been employed to model liquid solid systems: Lattice-Boltzmann simulations (Ladd and Verberg 2001), Direct Numerical Simulations (Glowinski, Pan et al. 1999), Two-fluid interpenetrating continua (Crowe 2012), Stokesian dynamics (Nitsche and Batchelor 1997; Pignatel, Nicolas et al. 2011) and Spectral Methods with particle tracking (Bosse, Kleiser et al. 2005).

When the particles are uniformly distributed in a homogenous dispersion, the mean velocity would be less than the terminal settling velocity of a single particle. This phenomenon is called hindered settling. Richardson and Zaki (1954) presented an expression that relates this hindered velocity of the suspension to the terminal settling velocity of the particle, u_0 and some function of the volume fraction of solids in the suspension, φ.

$$u_s = f(\varphi) * u_0 \qquad (2.1)$$

They determined $f(\varphi) = (1 - \varphi)^n$ where the exponent, n is close to 5 for small particle Reynolds numbers.

Batchelor (1972) focused on the theoretical determination of the mean value of the velocity of a sphere in a dilute suspension of identical spheres. In formulating the problem, the effect of inertia was neglected to preserve linearity of the system. If the probability distribution of a given configuration of particles is known we can determine the average of some quantity G associated with some position in the dispersion.

$$\bar{G} = \frac{1}{N!} \int G(x, \mathbb{C}_N) P(\mathbb{C}_N) d\mathbb{C}_N \qquad (2.2)$$

$\mathbb{C}_N$ is the configuration of a set of N identical particles and $P(\mathbb{C}_N)$ is the probability density of the configuration. The key result of the work was to determine the correction to the average settling velocity. This value was found to depend on the size, shape, particle density and concentration of the suspension and proposed a correction to the settling velocity to be $O(\varphi)$ in contrast to the $O(\varphi^{1/3})$ dependence. Accordingly,

$$f(\varphi) = 1 - 6.55\varphi + O(\varphi^2) \qquad (2.3)$$

The second term on the right hand side of equation 2.3 is due to the backflow of displaced fluid as the particles settle. There are difficulties in finding analytical solutions to the setting of a dispersion of particles: The slow decay of the velocity disturbance produced in a fluid by a settling sphere goes asymptotically as $1/r$ where r is the radius of the sphere; the random arrangement of particles in dispersion also makes calculations cumbersome. We can however overcome the difficulties of a rigorous analytical solution for sedimentation by employing an Eulerian-Lagrangian description of the flow. If the dispersion is described as a regular array of spheres (cubic, rhomboid etc.), the fractional reduction in fall speed is proportional to $\varphi^{-1/3}$ with

a constant of proportionality that depends on the arrangement used. Batchelor (1972) used a statistical-analytical approach to take into account the randomness of the configuration of particles in the dispersion.

He also pointed out that the difference between homogenous and inhomogeneous sedimentation is not in the presence or absence of rigid boundaries in the vicinity of the particles but the spatial variation of the statistical properties of the dispersion.

As opposed to hindered settling, a phenomenon which we could term "enhanced" settling occurs when a cluster of particles assumes a single identity thus causing the particles to settle many times faster than their individual terminal speed. Nitsche and Batchelor (1997) and Favier, Abbaspour-Fard et al. (2001) presented an expression validated by the experiments of Kohring, Melin et al. (1995) from theoretical analysis that is valid at low Reynolds number which shows the enhanced settling of a cluster of particles where the cloud velocity is u_c, the number of particles in the cloud is N and the ratio of the particle radius to cloud radius is ϵ:

$$\frac{u_c}{u_0} = \frac{6}{5} N\epsilon + 1 \tag{2.4}$$

A consequence of low Reynolds number is the slow particle leakage from the rear of a cloud. Nitsche and Batchelor (1997) investigated the breakup of a falling drop of particles within this limit. Multiple hydrodynamic interactions among particles cause random crossings of the imagined boundary of the blob – the loss of particles in the tail is a purely hydrodynamic effect. The Knudsen numbers are relatively high and thus no Brownian motion is involved in this random motion. The loss of particles in the tail of the blob is one mechanism in the smoothening out of the bulges that may have been present in the initial stages of sedimentation and may be an explanation why the breakup mechanism is not similar to that observed at higher Reynolds

numbers where secondary droplets develop from these bulges (Machu, Meile et al. 2001). The goal of their work was to observe the time evolution of a spherical blob and quantify the rate of leakage from the finite dispersion. They noted that the blob could fall in a manner resembling circulating halo of particles but without change to its compound spherical structure at low Reynolds numbers. A flux of particles across the interface of the cloud can be inferred from the leakage of particles as opposed to using a particle diffusivity of the conventional kind which would involve having an expression for the irregular surface of the blob. This can be modeled using Newton's law of motion to calculate the acceleration of the particles while the hydrodynamic forces on a single particle are calculated from the torque-free solution to the Stokes equation for N-1 number of spheres. Clusters of particles can be regarded as an effective continuum with a density higher than the surrounding fluid. The difficulty in using the Stokeslet approach as noted by Nitsche and Batchelor (1997) lies in the unrealistically large ambient fluid velocity that could be calculated when two particle centers overlap. One method of solving this problem is to impose an artificial short-range repulsive force on each particle to keep them apart. This arbitrary force may be unnecessary and may modify the flow-field in an undesirable way (Ekiel-Jezewska, Metzger et al. 2006). Despite this relatively simple approach, the basic toroidal feature of cloud sedimentation can be reproduced. The rate of particle leakage is directly proportional to the single-particle terminal settling speed and inversely to the mean particle spacing to the fourth, d^4, over a wide range of initial particle numbers.

$-dN/dt = const * u_0 R^2 a/d^4$ where R is the blob radius. This result is expected because the leakage rate should scale as the magnitude of the fluctuations, $O(u_0)$, and be related to the area available for transfer of excess mass, $O(R^2)$. Their simulations went up to a particle number of just 320 particles.

In a more recent paper, Pignatel, Nicolas et al. (2011) investigate the dynamics at small but finite

Reynolds number. In order to properly characterize the flow regime of the cloud, they define a

non-dimensional parameter which they call the "inertial length", l^* which quantifies the ratio of

viscous to inertia forces. $l^* = (a/R)/Re_p - a$ and R are the particle and cloud radiuses

respectively. The particle Reynolds number is defined as $Re_p = \rho U_0 a/\mu$ where the terminal

velocity of a single isolated particle is $U_0 = 2(\rho_p - \rho)a^2 g/9\mu$, g is acceleration due gravity and

μ is the liquid dynamic viscosity. On the basis of the inertial length, there are thus three

identifiable flow regimes – the Stokes cloud regime where both Re_c and Re_p are <<1 (Re_c is

Reynolds number of the cloud, $Re_c = \frac{\rho v_c R}{\mu}$, where $v_c = \frac{6}{5}U_o(N_p \epsilon + 1)$, $\epsilon = a/R$); the macro-

scale inertial regime where Re_c is no longer infinitesimal; micro-scale inertia regime (where both

Re_p and Re_c are not small). In the Stokes regime, pure hydrodynamic interactions are sufficient to

model the dynamics of the physical system.
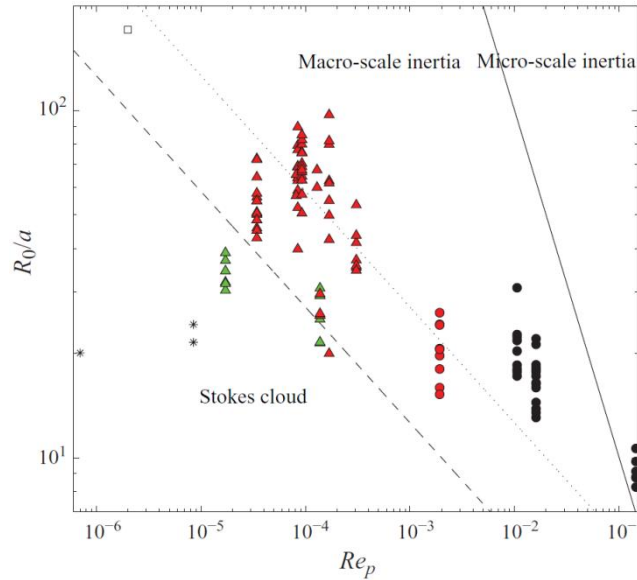
Figure 2.1: Three regimes of cloud settling based on particle and cloud scale inertia (Pignatel, Nicolas et al. 2011)

The particles can be treated as point forces and only far-field interactions are accounted for. The inertial length is highest in this regime. As we reduce the inertial length, we enter into the macro-scale inertia regime. The third and final regime, the micro-scale inertia regime deals with systems where both Re_c and Re_p are not negligible. Their studies focused on the last two regimes. By keeping the Stokes number ($St = \frac{2}{9}(\rho_p/\rho)Re_p$) roughly the same in the number of parameters to be studied can be reduced to Re_c, N and l^*. Pignatel, Nicolas et al. (2011) used a method of simulation called the Oseenlet simulations, which is a modification of the Stokeslet but contains an additional term to the steady state, reversible solution to flow around a sphere to model non-negligible inertia at long distances. Due to Oseen's approximation, the Oseenlet remains linear but upstream and downstream symmetry is lost. The linearity permits a summation of the hydrodynamic disturbance to the flow field from multiple momentum sources. The dynamics of cloud settling using this method were found to be in agreement with those in other studies. As the cloud descends circulation within the cloud structure, expansion and eventual breakup of the cloud occur. This series of events is consistent under most flow conditions with only slight variations for each flow regime. They observe no particle leakage when the inertial length is small but as the inertial length is increased (corresponding to a reduction in the associated Reynolds numbers), particle leakage becomes a more quantifiable phenomenon. One highlight of their conclusions is that the mechanism for torus formation depends on the flow regime. At low Re_c, particle depletion along the vertical axis of the cloud causes the formation of torus while in the former, inflow of fluid at the rear of the cloud is responsible. The difference between these 2 mechanisms is also what accounts for the absence of particle leakage at high Reynolds numbers as particles that would otherwise be lost in the wake of the descending cloud are conveyed back into the cloud by the recovering fluid. In addition, the

breakup observed in a non-inertial regime is different from that in a high inertia regime. The

cloud flattens as it descends, reaches a critical aspect ratio and loses its symmetry without

evolving first into an open torus in the former while in the latter (this validates earlier

experiments and simulations of Machu, Meile et al. (2001)), the fluid streamlines can pass

through the center of the cloud creating an open torus well before the amplification of bulges on

the torus and breakup.
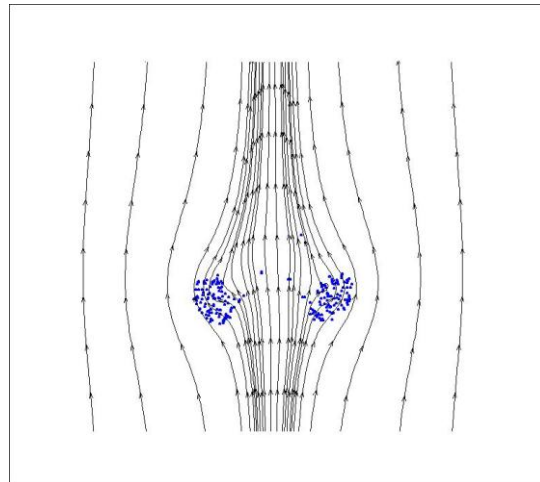
Figure 2.2 : Open Torus showing fluid streamlines passing through the center. Only particles in
the Meridien plane are shown for clarity

They define an aspect ratio as the diameter of the cloud in the horizontal direction to the

diameter in the vertical direction. The average settling velocity, growth of the aspect ratio of the

particle cloud and break-up time at low Reynolds number regimes matches the experimental

results presented but strong deviation is seen when the same comparisons are made at higher

Reynolds number and higher volume fractions. This may be due to the nature of the modeling

approach used which does not account for the effect of a finite particle volume and a possibility

of increased frequency of collisions.

The role of particle-particle interactions in shape evolution of a cloud of particles was explored by Metzger and Butler (2012) who considered the influence of periodic shear flow on a neutrally buoyant cloud of particles that were close to the packing limit for mono-size hard spheres. The question they wanted to answer was whether the cloud of particles deformed through shear strain on the host fluid regains its original configuration upon reversal of the flow. In order to completely eliminate the effects of inertia, the fluid used was highly viscous. Advection therefore plays no part in the evolution of the cloud and the sole cause of departure from the initial shape of the cloud is inter-particle effects. By setting up their experiments they also wanted to clarify the significance of non-hydrodynamic interactions in modeling rheology of suspensions. Two factors govern the irreversibility or otherwise of the system: If the strain amplitude is above a critical value, the flow is irreversible; also, a close packing of the cloud at the start of the operation would mean that there has to be a dilation of the particle cloud as two adjacent layers of particles slide past each other. Reversibility seemed to be a feature of configurations that had sufficiently dilated or those with low enough volume fractions. The process produced interesting "galaxy" like shapes indicating that the core of particles moved as one entity while particles on the periphery are dispersed. They conclude that the reversibility of the time evolution of a cloud under imposed shear occurs below certain threshold concentrations constrained by the shear rate of the characteristic background flow points to the strong relationship between irreversibility and particle-particle collisions. They point out that long-range hydrodynamic interactions are not the only sources of chaos in particulate systems

Mylyk, Meile et al. (2011) studied cloud destabilization in the presence of a hard vertical wall by performing experiments and stokes simulations. They found that the evolution of the cloud is fundamentally the same in an unbounded fluid but leakage is faster and the onset of

destabilization is quicker. Most of their blobs broke up into 2 secondary blobs with a few into 3 blobs. The destabilization time and length were measured qualitatively as the time and distance when the open torus or flattened blob begins to bend. Their most important result was to find a linear correlation between the two quantities and the distance between the cloud centroid and the wall for both experiments and simulations. The experiments showed a slightly more cohesive behavior than their point particle simulations and this can be attributed to the liquid bridging that exist in liquid solid systems.

Regardless of the initial shape of the cloud, at low to moderate Re_c, the torus is the only intermediate shape before the cloud disintegrates. Streamlines of fluids do not immediately pass through the center of the torus after its formation and due to the formation of a "stream envelope" that encloses the streamlines within the cloud structure even when only a low density of particles is present in the hole of the torus. After some time has elapsed, the fluid streamlines pass through the center of the torus to form an "open torus". This open torus is what is prone to disintegration. An explanation of the leakage of particles different from that presented by Nitsche and Batchelor (1997) is given. To explain the leakage of particles, they define a stream envelope as the imaginary surface separating the outer bypassing streamlines and the inner toroidal circulations within the cloud substructure.
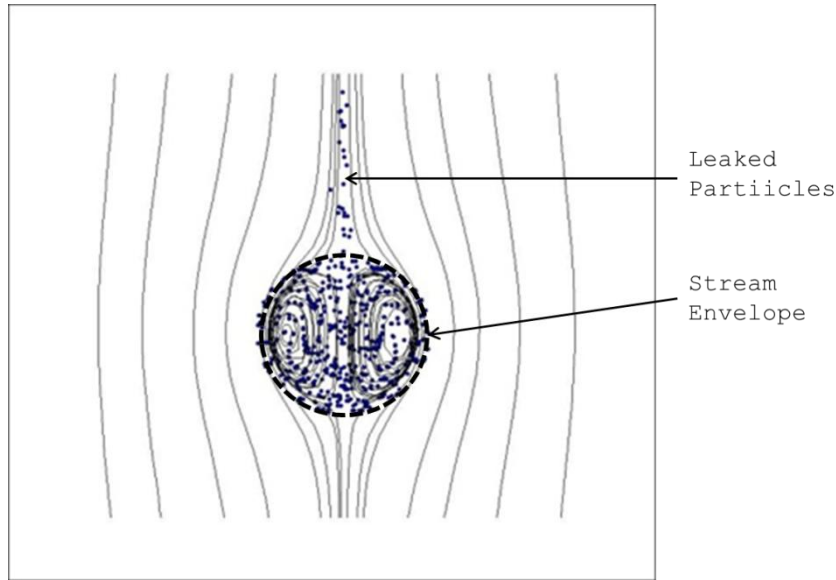
Figure 2.3: Stream Envelope at low Re_c

The envelope of closed streamlines extends partly outside the drop to permit recirculating

particles in the core of the cloud to entrain the bypassing streamlines and be swept to the rear of

the cloud and subsequently lost.

Using a spectral method for the fluid phase while tracking particles in a lagrangian framework,

Bosse, Kleiser et al. (2005) simulated the behavior of a settling cloud under a range of Re_c from

0 to 100. In all simulations they use the standard drag coefficient for the description of the drag

on each particle and the buoyancy force as the driving force of motion. Their Navier-Stokes

equation was modified by a feedback source term into the fluid phase for the motion of particles

with the source term applied at the particle centers. Other parameters explored by their

simulations include the stokes number of a single particle based on its terminal settling speed, the

Froude number on the scale of the cloud radius, Fr, and the ratio between the density of the solid

and continuous phase, ρ_p/ρ and the initial volume fraction of the blob, φ. The cloud Reynolds

number places a more stringent constraint on the extent to which inertial forces dominate the

system than does the particle Reynolds number and fixing this value as low to moderate ensured

they remained within a viscous dominated regime. Their simulations produced several interesting patterns for the shape evolution of the blob. For reasonably low Re_c, the blob retains its roughly spherical integrity and shows streamlines that enclose a vertical substructure within the blob. As they increased Re_c, the blob shows increasing tendency to disintegrate into 2 or more blobs which themselves disintegrate in a cascade of secondary drops. Their study showed the underlying transitional nature of the sedimentation of a particle blob. There was also an observed increase in the number of secondary drops with Re_c. They also exposed the role that the initial particle distribution plays in the ensuing instability. As long as perturbations to the initial spherical shape of the cloud are of the order of the mean particle spacing, different patterns can be triggered. Grid resolution was also mentioned as a possible mechanism for the number of secondary clouds produced.

Metzger, Nicolas et al. (2007) report that at low Re, if the velocity of settling is normalized by Stokes settling velocity, the velocity bears linear relationship with N^*/R^* where the normalized Number of particles is $N^* = N/N_0$ and normalized cloud radius is $R^* = R/R_0$. The rate of departure from the Hadamard Rybczynski streamlines was also studied and was found to scale as $N_0^{-1/3}$. They also observed different shape evolution for oblate and prolate clouds where oblate clouds possess a tendency to show instabilities by transitioning through tori while prolate clouds tend to leak particles more readily. The prolate shaped cloud recovers the spherical shape and then evolves into a torus at longer times. Finally, a criterion for destabilization is proposed for the class of clouds they studied based on a critical aspect ratio. The aspect

ratio, $\gamma = \dfrac{\sqrt{\sum_{i=1}^{K} f_i \cdot (x_i - \bar{x})^2}}{\sqrt{\sum_{i=1}^{K} g_i \cdot (y_i - \bar{y})^2}}$, (point $(\bar{x}, \bar{y})$ is the center of the cloud and point (x_i, y_i) is the location

of particle i while f_i and g_i are discrete probability distribution functions for particles in both the

x and *y* directions). They found that when the aspect ratio reaches a critical value

$(\gamma \geq \gamma_c = 1.64)$, and for particle number between 1000 and 3000, the cloud simulations predict

destabilization.

Swan and Brady (2011) showed that the nature of the boundary at the top wall affects the flow of

particles. If the suspension is entirely closed, the rate of sedimentation drops as a result of the

significant backflow that is generated by the fluid   as the suspension settles. In the case of a

channel that is left open such that fluid may flow freely into and out of the flow domain, the

suspension settles faster than when the fluid is confined such that there is no net flow into the

system.

Abade and Cunha (2007) were interested in the effect of polydispersity on the aggregated

behavior of settling clouds and velocity fluctuations. Their method of simulation was using point

particle stokeslets. They find that the lifetime of a blob with significant polydispersity is less than

that of a comparative mono-disperse blob. In order to get an expression for the rate of particle

leakage, they treat it as a continuum phenomenon by relating the flux of particles across the

imaginary surface of the blob to the fluctuation of particle velocity around a mean which is the

source of particles randomly crossing the imagined surface of the blob. Their result was an

exponential relation between the rate of particle leakage and the number of particles left in the

blob while it remains spherical as $-dN/dt \sim {}^{3}/_{4} N^{2/3} \epsilon^2$.

Davis and Acrivos (1985) studied the enhanced settling of particles due to inclined vessels. An

increase in the cross-sectional area available to the upward flowing fluid when particles form

layers of sediment on the wall leads to an increase in the sedimentation rate. They mention that

the settling velocity can be predicted from the thickness of the sediment layer, a sedimentation

Grashof number and a Reynolds number provided the flow is laminar and there are no instabilities in the form of waves in the flow.

Table 2.1: Brief summary of some of the important work that have been done on cloud settling

Ref	Experiment or Simulations	Method of Solution	Flow Regime	Phenomena Observed
Nitsche and Batchelor (1997)	E & S	Stokeslet	Stokes	Particle leakage
Pignatel, Nicolas et al. (2011)	S	Oseenlet	Micro and macro scale inertia	
Bosse, Kleiser et al. (2005)	S	Particle-tracking/spectral method	Stokes – macro scale inertia	Leakage, breakup
Metzger, Nicolas et al. (2007)	E & S	Stokeslets	Stokes	Leakage, Coalescence
Kohring, Melin et al. (1995)	E	Experiments	Stokes	Particle leakage
(Mylyk, Meile et al. 2011)	E & S	Oseenlet interactions	Macro-scale inertia	Break-up

2.1 Phases of Cloud settling

Despite the smaller degree of mixing compared to turbulent thermals, three distinct phases that resemble those of the descent of a thermal can be observed at moderate Reynolds number – a short period just after the release of the cloud that we would call the acceleration period in the manner of Rahimipour and Wilkinson (1992) where the motion of the cloud induced by gravity responds to the stationary background fluid through the drag this phase may be short depending on the Re_c of the particle cloud and is characterized by very little expansion of the cloud; A self-preserving phase where the general structure of the cloud remains axisymmetric either as an open or closed torus with internally circulating vortices within the cloud sub-structure with accompanying lateral expansion of the cloud; and finally a transition phase where the cloud losses its axisymmetric geometry and breaks up into any number of secondary clouds with subsequent dispersion into the host fluid.
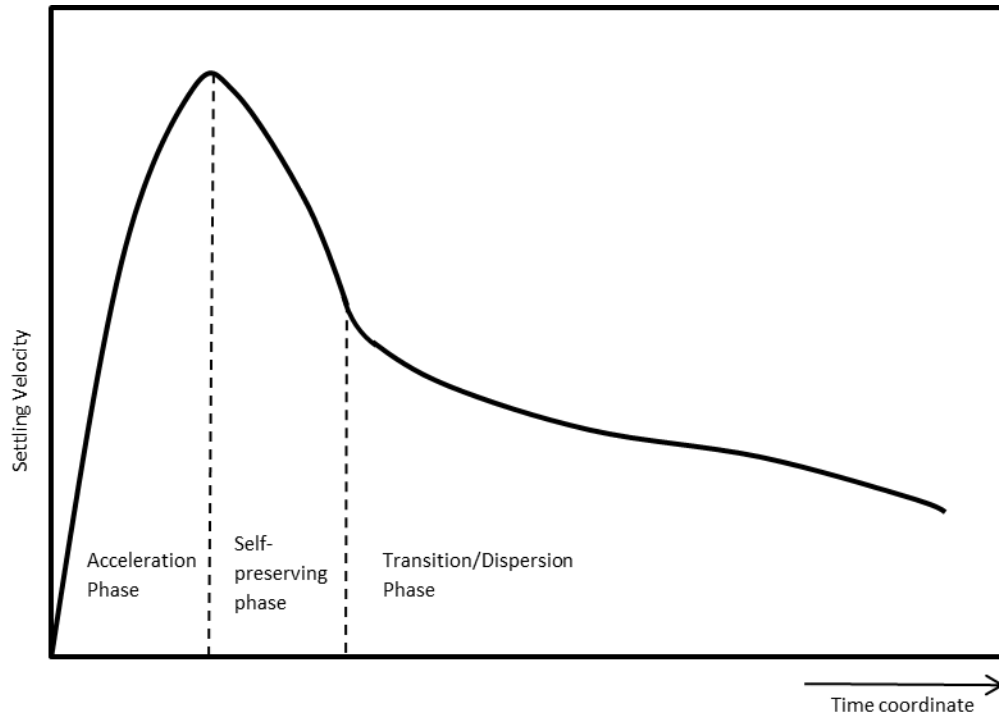
Figure 2.4: Cartoon depicting the stages of particle cloud evolution

2.2   Velocity Fluctuation

Of interest to researchers are the velocity fluctuations that arise in sedimenting systems. These

fluctuations are one of many observable quantities in studying the nature of hydrodynamic multi-

body interactions in liquid solid systems. A large body of literature is also devoted to the

interplay between the magnitude of velocity fluctuations and the system size. Caflisch and Luke

(1985) summed the hydrodynamic interactions of particles in a suspension and found that for a

suspension with uniform concentration throughout the system domain, the fluctuating velocity of

a test particle diverges indefinitely as we increase system size. This is at odds with the

experiments of Nicolai, Herzhaft et al. (1995) who found a saturation of the amplitude of

velocity variance at system sizes greater than $20a\varphi^{-1/3}$. One suggestion to bridge the theory and

experiment has been to try to identify methods by which the slowly-decaying $O(1/r)$

interactions are made to decay more rapidly. These so-called "screening" mechanisms have been the subject of research. Koch and Shaqfeh (1991) have suggested that these screening mechanisms can be modeled in the same fashion as the screening of electrostatic charges in an ionic liquid such that the neighborhood of a test particle is neutrally buoyant to the macro-scale suspension density. There have been attempts to explain the saturation of velocity fluctuations and the search for physical screening mechanisms that could make this occur. Brenner (1999) put forward a mechanism by which hydrodynamic screening can be achieved by keeping the probability distribution of particles random and making u decay faster than r^{-1}. He also makes the argument that the lifetime of particle clusters that appear in the system is important in determining the magnitude of the velocity fluctuations. The blobs in his simulations display certain features including stretching at initial times and swirling with the particles moving back and forth across the smallest dimension of the cell despite the low Reynolds number considered. Three-dimensional fluctuations were predicted despite the thin gap in one dimension of the cell. There was a dependence of the magnitude of fluctuations on the gap width. Particles near the wall displayed much smaller fluctuations than particles in the core of the blob.

Segre, Herbolzheimer et al. (1997) found that the velocity fluctuations will depend on the system size if the system size is less than the correlation length, ξ. The horizontal and vertical correlation lengths are defined as the lengths over which vertical and horizontal velocities are correlated respectively. They found the dependence of horizontal Correlation length on volume fraction to be $\xi_\perp = 27a\varphi^{-1/3}$ and the vertical correlation length to be $\xi_\parallel = 11a\varphi^{-1/3}$. These quantities are related to the swirl size in the suspension. They also found the amplitude of the vertical velocity fluctuations to be twice that of the horizontal velocity fluctuations.

Guazzelli and Hinch (2011) posited that long-range interactions between particles are observed at low Reynolds number cause disturbances in flow field of a test sphere of radius a and this and with a magnitude of $O(u_0 a / r)$. If the influence of other particles in the spherical region of radius R_c around a test particle is calculated summing the effects of their disturbances, the change in sedimentation velocity of the particle will be $O\left(\int \frac{u_0 a}{r} n dV\right) = O\left(u_0 \varphi \left(\frac{R}{a}\right)^2\right)$ where n is the number density of particles and V is the system volume. Settling velocity should therefore depend not only on the size but the shape of the container.

Kuusela (2005) studied the "steady state" characteristics of homogenous sedimentation. He was concerned with the "loss of memory" – a phrase coined to reflect the apparent chaotic nature of multi-body the particle fluid system – by tracking the velocity auto-correlation function as a function of time. By analyzing the integral of the velocity auto-correlation function over long time-scales, they were able to obtain values for horizontal and vertical self-diffusion. The latter were found to be higher. They found the velocity fluctuations to be sensitive to the size of the container and find that the spatial correlation length decreases with an increase in the volume fraction. Sangani and Acrivos (1982) calculated analytically the drag force when a fluid flows through a periodic or regular array of particles and find a linear dependence on $\varphi^{1/3}$.

Rubinstein and Torquato (1989) looked at the slow flow of a viscous fluid through a random array of particles by recasting Darcy's formula in an ensemble-averaged form and finding the upper and lower bounds for the permeability.

It is known that the correction to the Hadamard-Rybczinsky equation for the settling velocity of a suspension drop is $O(\varphi^{1/3})$ for an ordered suspension (Sangani 1987). However, a rigorous

theoretical analysis for the Stokes settling velocity of a drop for a dilute suspension with no regular configuration is not straight forward (Davis and Acrivos 1985).

2.3   Particle Clouds and Immiscible Liquid drops and their similarities

Machu, Meile et al. (2001) explore the similarities between liquid drops and particle clouds in both experiments and simulations and clarify that suspension drops have to contain a sufficient number of particles before they can approximate the behavior of liquid drops. Their simulation was done in the manner of Nitsche and Batchelor (1997) where gravity is the sole generator of flow field and the particles are modeled as stokeslets. They also point out the problem of the unrealistic velocity field due to the singularity in the stokeslet calculation resulting from the overlap of 2 or more particles. The nature of the stokeslet approach is such that because the point-force solution goes as r^{-1}, a singularity is generated as the centers of 2 particles approach. Unlike their predecessors, they do not employ any modification to the stokeslet to prevent this overlap but still end up with a reasonable flow field. Among some of the conclusions reached in their study was that the particle number influences the evolution into a torus.

3.0   Model Development

Liquid solid flows, in general, and the phenomena of leakage, torus formation and breakup in inhomogeneous sedimenting systems, in particular, have been simulated using different approaches. The two-fluid model, point-particles with Stokesian dynamics, Lattice-Boltzmann method, Direct Numerical Simulations, Euler-Lagrangian with Fourier pseudo-spectral formulation of the continuous phase are some of the solution methods that have been employed. In order to assess the instabilities in a deterministic way, we retain the Lagrangian description of the particulate phase and solve the fluid equation using the finite volume method.

3.1   Euler-Lagrange Discrete Element Method

The Euler-Lagrange method is a mesoscopic scale model that involves a continuum description of the fluid phase. Its application to particle-laden flows was popularized by the works of Tsuji, Kawaguchi et al. (1993), Hoomans, Kuipers et al. (1996). The nomenclature of this method comes from the fact that the continuous phase equation is solved using the volume-averaged Navier Stokes equations while the discrete phase is solved using the net force on the individual particles as predicted by the Newton's law of motion for a rigid body. Unlike direct numerical simulations (DNS) where the flow around the particle is fully resolved, (Hu, Joseph et al. 1992; Glowinski, Pan et al. 1999; Veeramani, Minev et al. 2007) here the focus is on sub-grid particles whose size is smaller than the smallest computational cell. Wu, Berrouk et al. (2009) note that even though the flow around the particles is not well resolved, many important features of fluid-particulate flows are reasonably captured by such a procedure. The large structures observed in multiphase flows like torus formation in a sedimenting cluster of particles (as shown in this work) and bubble formation in fluidized beds are directly influenced by particle-fluid and particle-particle interactions despite the huge scale separation (Deen, Annaland et al. 2007). The

computational cost of this method by comparison to DNS is lower and it represents and intermediate stage of multiphase flow modeling between the Euler-Euler two-fluid method (TFM) and DNS. It is thus suitable in providing enough information to enhance modeling of hydrodynamic, interpenetrating continua models.

Figure 3.1: Hierarchy of the computational cost of various models used in dispersed flow modeling.

The result of this DPM procedure is that the particles are tracked discretely while the overall effect of particles within a given computational cell is averaged and returned to the Navier-Stokes equation as a source term.

3.2 Comparison of Time-driven and Event-driven solution Strategy

The hard sphere model, first proposed by (Campbell and Brennen 1985) involves first the detection of the "event" of particle-particle contact before the subsequent calculation of the pairwise rotational and translational moments. It is hence widely described as an event-driven solution strategy. It involves tracking the nearest-neighbor instantaneous particle interactions treated only as binary collisions. The hard sphere model has been successfully employed in literature to model gas-solid flows. The major drawback of this strategy has been the fact that it is not amenable to parallelization even though for dilute systems, hard sphere model is a faster strategy. (Deen, Annaland et al. 2007) has given a comprehensive review of the hard sphere model.

The soft-sphere model on the other hand first proposed by Cundall and Strack (1979) is capable

of handling ternary or greater particle collisions. The net contact force on each particle is

however calculated based on a vector sum of all the pairwise interactions on the particles (Deen,

Annaland et al. 2007). Because the interaction between particles is calculated using information

about the overlap of particles, and one only needs to add this as a force in the particle dynamic

equation, this strategy yields itself to parallelization. It is called time-driven because one does not

need to worry about first explicitly detecting collisions before the impulse is imposed on the

dynamics of the particle. One needs to only worry about the size of the time-step to prevent

large, unphysical overlap between particles. This therefore means that we are able to observe not

only the short range forces that result from direct particle contact but also long-range influence

of particles not in direct contact.

3.3   Governing Equations

3.3.1   Fluid Phase – Volume Averaging

If we define a given property, ψ of a multiphase system, in order to model this property it may be

impracticable to track this property over every position for every phase within the flow domain

exactly. The concept of volume averaging is to deal with the quantity by relating it to the volume
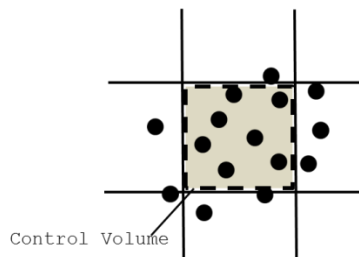
fraction of each phase.

Figure 3.2: Illustration of a suitable control volume

The control volume should not be too small in order to ensure that the average doesn't vary with the size of the averaging volume and it should not be too large that it can no longer provide a reliable local value for ψ.

The averaging of any top-level equation in fluid dynamics results in terms for which appropriate closures must be found. The fluid motion in coupled CFD-DPM/DEM models is governed by the volume-averaged continuity equation which balances the flux of material with the material within the control volume:

$$\frac{\partial}{\partial t}(\varepsilon\rho) + \nabla \cdot (\varepsilon\rho\boldsymbol{u}) = 0 \qquad\qquad 3.1$$

The fluid phase density, ρ and velocity, $\boldsymbol{u}$, are defined. The volume fraction of the fluid phase is represented by ε.

In addition, the volume-averaged Navier Stokes equation is given as:

$$\frac{\partial}{\partial t}(\varepsilon\rho\boldsymbol{u}) + \nabla \cdot (\varepsilon\rho\boldsymbol{u}\boldsymbol{u}) = -\varepsilon\nabla p + \nabla \cdot (\varepsilon\tau) + \boldsymbol{S} + \boldsymbol{S}_a + \varepsilon\rho\boldsymbol{g} \qquad\qquad 3.2$$

Where p is the static pressure, τ is the stress tensor and $\boldsymbol{g}$ represents the acceleration due to body forces namely gravity. $\boldsymbol{S}$ is the momentum source due to the interphase drag term and comes from averaging of the original Navier-Stokes equation. Appropriate models are used to close this term and some of these models would be presented shortly. As presented in (Goldschmidt, Beetstra et al. 2004), the source term which is computed by the volume-weighted summation is modeled as follows:

$$S = -\frac{1}{V}\sum_{k=1}^{N_P} \frac{V_{p,k}\beta}{1-\varepsilon}(u - u_{p,k})\delta(x - x_{p,k}) \qquad 3.3$$

Since the particles are smaller than the computational cell, a smearing of the discrete momentum sources at the Lagrangian particle positions unto the computational cell must be performed. This is accomplished by weighting the momentum source calculated at the center of the particles located in a given cell with the volume of the particles that intersect with the computational cell.

There are several correlations used in literature to model the interphase momentum transfer coefficient, β and provide appropriate closure for equation 3.2. Among those explored in this work are as follows:

Syamlal & O'Brien:

$$\beta = 0.75 \frac{\varepsilon\varepsilon_p \rho}{d_p v_r^2} C_D |u_p - u| \qquad 3.4$$

Where $\varepsilon_p = 1 - \varepsilon$

$$C_D = \left(0.63 + \frac{4.8}{\sqrt{Re_p/v_r}}\right)^2 \qquad 3.5$$

$$Re_p = \frac{\rho|u - u_p|d_p}{\mu} \qquad 3.6$$

The correlation, v_r, is based on Richardson and Zaki (Richardson and Zaki 1954)

$$v_r = \frac{1}{2}\left(A - 0.06Re_p + \sqrt{(0.06Re_p)^2 + 0.12Re_p(2B - A) + A^2}\right) \qquad 3.7$$

$$A = \varepsilon^{4.14} \qquad 3.8$$

$$B = \begin{cases} 0.8\varepsilon^{1.28} & \varepsilon \leq 0.85 \\ \varepsilon^{2.65} & \varepsilon > 0.85 \end{cases} \tag{3.9}$$

Kuipers Wen & Yu (Wen 1966) correlation for high porosities ($\varepsilon > 0$).

$$\beta = \frac{18\mu}{d_p^2} F_c |u_p - u| \tag{3.10}$$

Where $F_c = \frac{10\varepsilon_p}{\varepsilon} + \varepsilon^3 \left(1.0 + 1.5\sqrt{\varepsilon_p}\right) + \frac{C_D}{24\varepsilon}$, $C_D = \frac{0.413\left(\frac{Re_p}{\varepsilon} + 3\varepsilon_p \varepsilon Re_p + 8.4 Re_p^{0.657}\right)}{1.0 + 10^{3\varepsilon_p}/Re_p^{(0.5+2\varepsilon)}}$

3.4 Two-way Coupling

In multiphase systems we need to model the interaction between all the phases. The exchange of momentum is of primary concern here but other types of interactions including the exchange of mass, energy might be important in other systems.

The type of coupling to be considered for the particle and fluid motion depends on the flow regime. The Stokes response time, τ_p is one parameter used to determine what flow regime we are in and it quantifies the response of the particle to the continuous phase flow field.

$$\tau_p = \frac{2\rho_p a^2}{9\mu} \tag{3.11}$$

The ratio of the fluid dynamic response time of the particle to the characteristic time scale of the flow is called the Stokes number and governs the nature of particle fluid coupling. In the case of a settling blob of particles the time scale of the flow is generally taken as R/u_c (Nitsche and Batchelor 1997; Machu, Meile et al. 2001; Bosse, Kleiser et al. 2005). R is the initial radius of the blob and u_c is a velocity of the order of the cloud settling speed and is typically $\left(\frac{6}{5}N\epsilon + 1\right)u_0$ for low Reynolds numbers. The Stokes number is therefore

$St = \tau_p \frac{u_c}{R} = \frac{2}{9} \frac{\rho_p}{\rho} \epsilon^2 Re_c$. If *St* is high, it means that the particle inertia is too great to be

affected significantly by the fluid stream. If *St* is low, it means the response of the particle to

changes in the continuous flow equation is instantaneous therefore supporting a one-way

coupling provided the volume fraction is low.
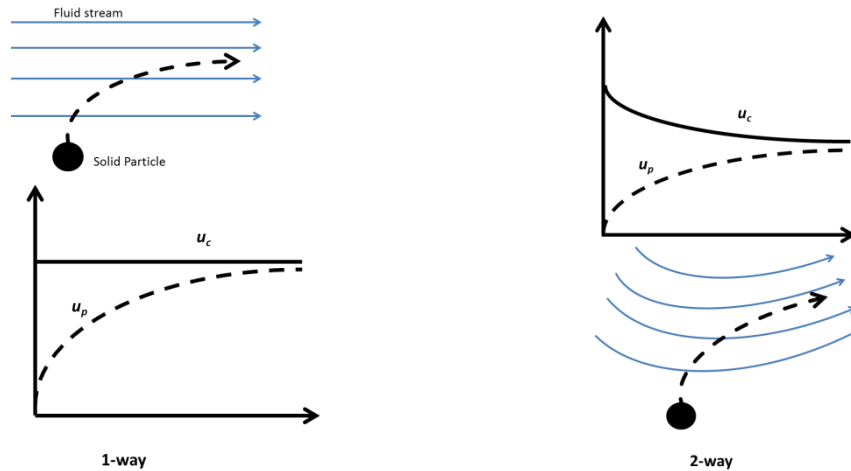
Figure 3.3: Illustration of one-way and two-way coupling

The value of the volume fraction would determine the kind of solution approach that would be

suitable to the physical system. For low volume fraction dispersion we can opt to use the discrete

phase particle tracking approach. For high volume fraction and high Reynolds numbers where

particle-particle dynamics become important because of inter-particle contacts, it would become

important to include the effect of volume fraction in the phase interaction and particle dynamics

3.5   Particle Dynamics

The governing equations for the dispersed phase follow the rigid body dynamics for a sphere or

point particle.

$$\frac{du_p}{dt} = F_D(u - u_p) + \left(1 - \frac{\rho}{\rho_p}\right)g + \frac{F_a}{m_p} \qquad 3.12$$

The second term is the buoyancy force per unit particle mass resulting from the displacement of

fluid of the same volume as the particle. F_a is the net force on the particle and can be a

combination of several additional forces depending on the particle fluid system of interest. These

include the far-field pressure gradient and the drag force resulting from the relative motion of

two phases.

$$F_a = -V_p \nabla p + F_D(u - u_p) + F_{contact} \qquad 3.13$$

In the case of high volume fraction a four-way coupling procedure necessary to include the

short-range particle-particle collision forces hence the third term.

3.5.1 Dilute Regime

For a volume fraction <0.1, the solution can be modeled without accounting for the volume

fraction in the two-way coupling term in order to improve the efficiency of the simulation. The

approach is based on the Particle-Source-In-Cell method proposed by Crowe, Sharma et al.

(1977). It does not account for the dispersed phase volume fraction nor particle-particle

interactions. This method is used where we intend to explore the minimum physics required to

model solid-liquid flows and the range its range of applicability within the context of

sedimentation. Accordingly, $F_D = \frac{18\mu}{\rho_p d_p^2} \frac{C_D Re}{24}$ where $Re = \frac{\rho_p d_p |u_p - u|}{\mu}$ and C_D is the drag

coefficient. The treatment of C_D is can be treated based on the value calculated using Stokes

drag, $C_D = 24/Re$ or the standard drag law, $C_D = \begin{cases} if \ Re_p \geq 1000, \quad C_D = 0.44 \\ if \ Re_p < 1E - 20, \quad C_D = 1.0E20 \\ otherwise \ C_D = \frac{24}{Re_p}(1 + 0.15Re^{0.687}) \end{cases}$.

29

3.5.2   Dense Regime

For high volume fractions, a different strategy is employed in modeling the dispersed phase. The drag term should be modeled to include effects of volume fraction $F_D = \frac{\beta}{1-\varepsilon}$ where β would also depend on the volume fraction and can be modeled based on the several available drag laws.

Syamlal & O'Brien

$$\beta = 0.75 \frac{\varepsilon \varepsilon_p \rho}{d_p v_r^2} C_D |u_p - u| \qquad\qquad 3.14$$

Where $\varepsilon_p = 1 - \varepsilon$, $C_D = \left(0.63 + \frac{4.8}{\sqrt{Re_p/v_r}}\right)^2$. The correlation, v_r is based on Richardson and

Zaki (1954):

$$v_r = \frac{1}{2}\left(A - 0.06Re_p + \sqrt{\left(0.06Re_p\right)^2 + 0.12Re_p(2B - A) + A^2}\right), A = \varepsilon^{4.14},$$

$$B = \begin{cases} 0.8\varepsilon^{1.28} & \varepsilon \leq 0.85 \\ \varepsilon^{2.65} & \varepsilon > 0.85 \end{cases}$$

Wen & Yu

Wen (1966) correlation for high porosities (ε>0.8):

$$\beta = \frac{3}{4} C_D \varepsilon_p \frac{\rho}{d_p} |u - u_p| \varepsilon^{-1.65} \qquad\qquad 3.15$$

The drag coefficient for an isolated particle is given by Rowe and Henwood

(1961): $C_D = \begin{cases} \frac{24}{Re_p}\left(1 + 0.15Re_p^{0.687}\right) & if\ Re_p < 1000 \\ 0.44 & if\ Re_p \geq 1000 \end{cases}$

Ergun correlation (Ergun 1952)

$$\beta = 150 \frac{\varepsilon_p^2}{\varepsilon} \frac{\mu}{d_p^2} + 1.75\varepsilon_p \frac{\rho}{d_p} |u - u_p|$$

Gidaspow (1994) combines the Wen and Yu correlation with the Ergun equation:

$$C_D = \begin{cases} \beta_{Wen\ \&\ Yu} & when\ \varepsilon > 0.8 \\ \beta_{Ergun} & when\ \varepsilon < 0.8 \end{cases}$$

The second consideration for dense particulate flow would be the collision dynamics that must

be incorporated into the solution. The contact forces include the normal and tangential forces on

the particle by other particles. The linear spring, dashpot and friction slider model of Cundall and

Strack (1979) is employed.
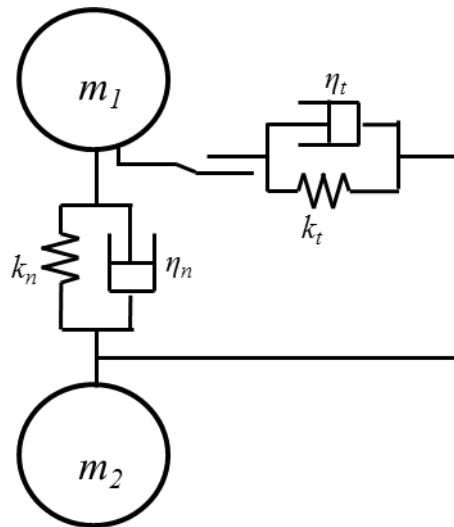
Figure 3.4: Spring-dashpot-friction slider model

The resulting dynamic relationship between the normal forces in the spring-dashpot-friction

slider system result in a 2nd order ordinary differential equation

$$m_{eff} \ddot{\delta}_n = -k_n \delta_n - \eta_n \dot{\delta}_n$$

3.17

The effective mass of each of a particle pair is calculated as $\frac{1}{m_{eff}} = \frac{1}{m_1} + \frac{1}{m_2}$. The model

development follows from (Van der Hoef, Ye et al. 2006):

31

$$F_{contact} = F_{ab,n} + F_{ab,t} \qquad\qquad 3.18$$

$$F_{ab,n} = -k_n \delta_n n_{ab} - \eta_n u_{ab,n} \qquad\qquad 3.19$$

Where k_n is the normal spring constant, n_{ab} unit normal vector at the point of contact, δ_n is the overlap between the two particles and should not exceed 1% of the particle radius η_n is the normal damping coefficient

$$\delta_n = r_a + r_b - |x_a - x_b| \qquad\qquad 3.20$$

r_a and r_b are radii of the contacting particles while x_a and x_b are the positions of the particle centers. $\eta_n = 2\sqrt{\frac{m_{eff}k_n}{\pi^2 + \ln^2 e_n}} |\ln e_n|$. The unit normal vector, $n_{ab} = \frac{x_{ab}}{|x_{ab}|}$, the relative velocity,

$u_{ab} = u_a - u_b + (r_a\omega_b + r_b\omega_a) \times n_{ab}$, where $u_{ab,n} = (u_{ab} \cdot n_{ab})n_{ab}$.

In like manner, the tangential contact forces for the particle forces follow the argument for the

normal forces: $F_{ab,t} = \begin{cases} -k_t\delta_t - \eta_t u_{ab,t} & if\ |F_{ab,t}| \le \mu_f|F_{ab,n}| \\ -\mu_f|F_{ab,n}|t_{ab} & if\ |F_{ab,t}| > \mu_f|F_{ab,n}| \end{cases}$. k_t is the tangential spring

constant, $u_{ab,t}$ tangential relative velocity at the point of contact, δ_t is the tangential displacement, η_t is the tangential damping coefficient and μ_f is the coefficient of friction.

$u_{ab,t} = u_{ab} - u_{ab,n}, t_{ab} = \frac{u_{ab,t}}{|u_{ab,t}|}$. We calculate the tangential displacement between two

particles by deducing it from their relative tangential velocities: $\delta_t = \delta_{t0} + \int_{t_0}^{t} u_{ab,t}dt$. The

normal and tangential damping coefficients are calculated from the material properties such as

the coefficients of normal and tangential restitution, Young's modulus and the Poisson ratio

depending on the model used.

3.5.2.1 Linear Spring, dashpot and friction slider

In this model, the effective k_n and k_t for a particle pair is simply taken as the arithmetic mean of their individual springs stiffness's: $k_n = 0.5(k_{n,a} + k_{n,b})$. Likewise, $k_t = 0.5(k_{t,a} + k_{t,b})$. These expressions can be used without modification to calculate the contact forces in equation (contact force equation).

3.5.2.2 Non-linear Hertzian Model

It is expected that an increase in overlap of the colliding particles should result in an increase in area of contact. This obviously leads to the logical conclusion that there should in practice, exist a non-linear expression for the spring stiffness and the contact force. As stated in the literature (Muthukumar and DesRoches 2006), the contact force in this model bears a non-linear relationship with the overlap between the two particles and a non-linear spring stiffness. Equation 3.19 is modified as follows:

$$F_{ab} = -(k_{ab,n}\, n_{ab} - \eta_{ab,n} u_{ab})\delta_n^p \qquad\qquad 3.21$$

The exponent, p, is usually taken as 3/2. $k_{ab,n} = \dfrac{E_a E_b \sqrt{r_{eff}}}{E_a\left(1-\vartheta_a^2\right) + E_b\left(1-\vartheta_b^2\right)}$. Where the effective particle radius is $r_{eff} = \dfrac{r_a r_b}{r_a + r_b}$. E_a, E_b, ϑ_a and ϑ_b are the Young's modulus's and Poisson ratios of the two particles of interest respectively. The damping constant is given as $\eta_{ab} = \dfrac{3 k_{ab,n}\left(1 - e_{ab,n}^2\right)}{4|u_{ab}|}$.

3.5.2.3 Contact Time

An issue of interest in soft sphere modeling of discrete particles is the time of contact and how it affects the choice of the time-step in the numerical implementation. The solution to equation (spring-dashpot-slider equation) if recast in 1-dimensional space is given in Van der Hoef, Ye et al. (2006)

$$\delta_n(t) = \frac{u_{ab,0}}{\Omega} \exp(-\Psi t) \sin(\Omega t)$$

3.22

$$\dot{\delta}_n(t) = \frac{u_{ab,0}}{\Omega} \exp(-\Psi t) * (-\sin(\Omega t) + \cos(\Omega t))$$

3.23

Where $u_{ab,0}$ is the initial relative velocity and $= \frac{\eta_n}{2m_{eff}}$; $\Omega = \sqrt{\Omega_0^2 - \Psi^2}$ and $\Omega_0 = \sqrt{\frac{k_n}{m_{eff}}}$. If the

equation for the overlap is set to zero ($\delta_n = 0$) the duration of contact, $t_{contact}$ can be obtained.

$$t_{contact} = \frac{\pi}{\Omega}$$

3.24

It is important from a computational standpoint to properly choose the value of the DEM time-step at least half this value so that the calculation of the overlap would not be unphysically large. Key to this is our choice of the material properties k_n and k_t (Van der Hoef, Ye et al. 2006). Van der Hoef, Ye et al. (2006) also mention that the values of k_n and k_t chosen could purely reflect a need to keep the particle overlap to a reasonable fraction of the particle radius rather than to ensure rigorous modeling of the inter-particle interactions.

The net torque acting on a particle j with radius r_a is given as:

$$T = \sum_j r_a n_{ij} \times F_{ij,t}$$

3.25

In order to justify the addition of the added mass force, density ratio must be low: $\rho_p/\rho \ll 1$. This was not the case for the suspensions studied and in order to improve computation efficiency, this effect was not included.

3.6   Discretization

The finite-volume method is used for the spatial discretization of the volume-averaged equations of motion. In order to model the DEM-CFD method the first instinct is to reorganize the volume averaged equations of motion to look like those of the single-phase equations of motion with a source term that can be easily plugged into a commercial CFD solver like fluent, i.e.:

$$\frac{\partial \rho}{\partial t} + \nabla(\rho u) = S_c \qquad\qquad 3.26$$

And the momentum equation becomes:

$$\frac{\partial}{\partial t}(\rho u) + \nabla \cdot (\rho u u) = -\nabla p + \nabla \cdot (\tau) + \rho g + S_m \qquad\qquad 3.27$$

Where $S_c = -\frac{\rho}{\varepsilon}\left(\frac{\partial \varepsilon}{\partial t} + u \cdot \nabla \varepsilon\right)$ while the momentum source term is $S_m = S_c u + \frac{1}{\varepsilon}\left(S_p + \tau \cdot \nabla \varepsilon\right)$.

The source term resulting from interaction with the discrete phase is $S_p = S + S_a$. The source term can thus be applied into the commercial CFD solvers like FLUENT, Star-CD, CFX and Open-FOAM where the source terms can be calculated implicitly with other flow variable like the velocity field and pressure field calculation. However because this implementation is not based on the integral form of the governing equations they cannot be relied upon to guarantee mass balance and the discretization should begin not from the differential form of the governing equations but from other integral momentum and mass balance (Wu, Nandakumar et al. 2011). If we consider a general property ψ and write the transport equation for two-phase flow we have

$$\frac{\partial}{\partial t}(\varepsilon \rho \psi) + \nabla \cdot (\varepsilon \rho u \psi) = \nabla \cdot (\varepsilon \Gamma \nabla \psi) + s_\psi \qquad\qquad 3.28$$

Γ is the diffusivity. If we integrate over a control volume ΔV and reorganizing the equation to yield a new implementation of the source term

$$\frac{(\rho\psi)^{n+1} - (\rho\psi)^n}{\Delta t}\Delta V + \sum_f \psi_f \Lambda_f = \sum_f D_f + S_\psi \Delta V \qquad 3.29$$

The source term, S_ψ is $S_\psi = -\frac{1}{\Delta t}(\rho\psi)^n(1 - R_t) + \frac{1}{\Delta V}\sum_f(1 - R_f)(\Lambda_f \psi_f - D_f) + \frac{S_\psi}{\varepsilon_p^n}$. The

indexes $n+1$ and n indicate the current and previous time levels respectively. The diffusive flux,

$D_f = \Gamma_f(\nabla\varphi)_f \cdot A_f$, the convective flux, $\Lambda_f = \rho u_f \cdot A_f$, the "void fraction temporal ratio" and

"void fraction spatial ratio" at cell face are defined $R_t = \varepsilon_p^n/\varepsilon_p^{n+1}$ and $R_f = \varepsilon_f^{n+1}/\varepsilon_p^{n+1}$. An

accurate calculation of the void fraction gradient especially at the cell face is necessary to ensure

mass conservation (Wu, Nandakumar et al. 2011). Even though the system of interest is a closed

system where the calculation of the overall net flux is not critical to a meaningful result as with a

fluidized bed, Wu, Nandakumar et al. (2011) note that this solution strategy can help in

enhancing solution convergence.

The discretized momentum equation in direction i is given in the following form:

$$\bar{a}_p u_{i,P} = \sum_{nb} \bar{a}_{nb} u_{i,nb} + \varepsilon \sum_f^{NF} p_f A_i + S_i \qquad 3.30$$

$\bar{a}_p$ contains the coefficient of the fluid velocity in the expression of the source term hence

ensuring the implicit calculation of the momentum source. If the pressure field and face mass

fluxes are known, the velocity field can be obtained. We can't know the pressure field

beforehand because it is coupled to the velocity field. The collocated grid algorithm of Rhie and

Chow (1983) where both the pressure and velocity field values are stored at the cell center means an accurate method for calculating the face values should be used.

A first-order implicit scheme was used for temporal discretization.

The pressure-velocity coupling is handled in a segregated fashion by employing the SIMPLE algorithm. A pressure field is guessed and used to obtain a first estimate of the velocity field. This velocity field is used to constitute a system of equations for the domain from the continuity equation called the pressure correction equation. The pressure correction is then used to obtain a more accurate estimation of the pressure and velocity field and pressure field. The Algebraic multi-grid method is applied to the pressure correction equation.

3.7   Source Terms and Numerical Stability

The flow variables except the source terms are calculated implicitly. The source term is linearized and treated in a "semi-implicit" fashion.

$$S^{n+1} = A^n u^{n+1} + B^{n+1} \qquad\qquad 3.31$$

A^n is given as $A^n = -\sum_{k=1}^{NPC} V_{p,k}\beta^n/V$ and $B^{n+1} = \sum_{k=1}^{NPC} V_{p,k}\beta^n u_{p,k}^{n+1}/V$. B^n depends on u.

Therefore, in order to linearize the source term, β is calculated at the previous time-step hence the semi-implicitness. It can be seen that the value of magnitude of A^n is always positive when added to the coefficient of $u_{i,p}$ in the discretized equation. It therefore preserves convergence as it makes the system of equations for solving the velocity field more diagonally dominant and hence improving solution convergence.

In order to calculate the face centered value of the field variables, a second-order upwind differencing scheme is used.

$$\varphi_f = \varphi_{r,upwind} + \nabla\varphi_{r,upwind} \cdot dr \qquad\qquad 3.32$$

The numerical stability of the source term calculation especially for strongly coupled systems with high volume fraction must include the use of underrelaxation factor, α (Kohnen, Ruger et al. 1994) which is between 0 and 1.

$$S = S_{old} + (1 - \alpha)S_{new} \qquad\qquad 3.33$$

The value of the under-relaxation does not affect the accuracy of the final converged solution; this is controlled by the specified tolerance, time-step and degree of coarseness of the spatial discretization.

3.8   Implementation In Fluent

Fluent is an industry standard software used primarily for solving fluid flow. It hosts options for solving the mass, momentum, energy and species transport equations. The multiphase flow models implemented in fluent include the two-fluid model, Volume of fluid model, discrete phase model and the mixture model. The in-built discrete phase model is compared to the DEM model used in this work. The discrete phase model explicitly tracks the dispersed phase and can handle high mass loading but not high volume fractions and high particle collisions.

Because the density ratio between the liquid and solid phase is $O(1)$, the momentum coupling has to be handled implicitly. Fluent allows for a straight-forward implementation of the momentum source term using a user-defined interface written in C. Fluent like many other flow solvers is not designed to handle the specifics of every flow problem and hence allows for the customization of boundary conditions, material properties and sources and sinks in the governing physical equations. Due to the tight coupling between the pressure and velocity terms in the SIMPLE algorithm, the pressure field must be calculated implicitly. The source terms must be

linearized and coefficients absorbed into matrix of the coefficients of the cell centered velocities. The source terms must be related to the void fraction and the gradients of the void fractions on each cell especially for dense particulate flows. Fluent allows for the storage of additional cell properties like the void fraction as User-defined scalars and automatically calculates their gradients.

There are two time layers to be considered in the solution of any DPM-CFD problem: the fluid time-step, Δt and the DPM time-step, Δt_{DPM} which should be at least one order of magnitude smaller than the fluid time-step. The stiffness of the system of equations to be solved is by a first approximation $O\left(\frac{\Delta t}{\Delta t_{DPM}}\right)$. In order to preserve computational efficiency, this ratio must not be set too high but allowance should be made so that it is not too low as to result in unrealistic overlap between particles and unnatural values for the inter-particle forces. At the beginning of the iteration, the particles are assumed fixed in space and the volume fraction and its gradient are calculated. A bulk of the computational time is spent in the volume fraction calculation and hence it is calculated only once per fluid time-step. The particles are advanced in time using the rigid body equations and accounting for the drag and particle-particle interactions. The source terms are calculated based on the slip velocity of the particle relative to the fluid phase and the fluid phase momentum equation is solved by the flow solver. Selection of the time-step should be $O(1)$ less than the particle response time to accurately model the particle response to the fluid(Wu, Berrouk et al. 2009). The particle response time is given as: $\tau_p = \frac{\rho d_p^2}{18\mu}$. An advantage of the time-driven soft-sphere modeling strategy is that we do not need to wait till the end of the calculation of the fluid flow equations to calculate the particle interactions unlike the hard-sphere model. The particle equations can be solved alongside the fluid equation with the inter-particle

forces integrated over time. This permits us to use the domain decomposition for parallel computation. The work flow (figure 3.4) for the coupled DPM-CFD procedure is generic for both dense particulate flow (where volume fraction and collision effects are modeled) and dilute flow ($\varphi \leq 0.1$) and reflects the implicit coupling of both phases.

3.9   Initial and boundary Conditions

Except where otherwise stated, the initial particle distribution is in a regular lattice with the inter-particle separation defined as $\left(V_p/\varphi\right)^{1/3}$ where V_p is the volume of the particle. The boundary conditions used except otherwise noted is the impenetrable wall BC.

The physical model consists of mono-disperse micron sized particles, the continuous phase is an incompressible Newtonian fluid.
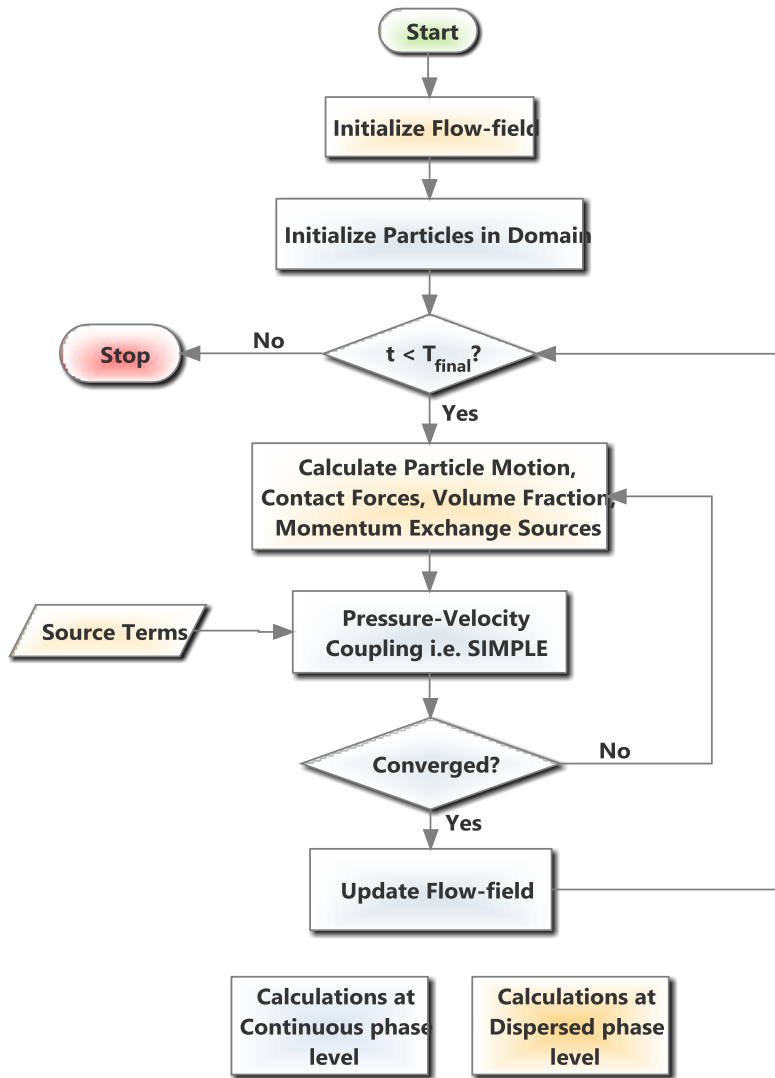
Figure 3.5: Solution algorithm flow chart

4.0   Results and Discussion

4.1   Validation

The descent of the cloud was validated both qualitatively and quantitatively. The cloud displayed the evolution and transition that is known to occur at low and moderate numbers. At low Reynolds numbers cloud deformation is not pronounced but cloud evolution is primarily due to the leakage of particles from the rear of the cloud. At higher Reynolds number, the evolution of the cloud is first into an axisymmetric torus and subsequently the breakup of the cloud into any number of secondary blobs depending on the discretization (number of particles in each realization of the cloud) and the flow conditions. We shall present some qualitative results in the subsections that follow. We first proceed to reproduce the volume fraction dependence at low volume fractions and low Re_c, particle leakage at low Re_c and torus formation and breakup at moderate Re_c.

4.1.1   Volume Fraction Effect and Enhanced Settling

One typical characteristic of sedimentation is that the settling speed of particles is altered as a result of long (hydrodynamic) and short range (contact) forces from that of the isolated particle. In the case of inhomogeneous settling, the particles' decent speed is enhanced as the cloud takes on a collective identity. The enhancement factor of the particle velocity is $O(\varphi\epsilon^{-2})$ and is therefore directly proportional to the number of particles in the discretization and the inter-particle spacing taking into account the particle size. The fall speed is dependent on the volume fraction of the cloud of particles, the density ratio ρ_p/ρ and viscosity of the host fluid. In the region of low volume fraction and low inertia, the settling speed has been determined through

42

asymptotic analysis (Nitsche and Batchelor 1997) and analytical solutions (Ekiel-Jezewska,

Metzger et al. 2006) and experiments (Alabrudzinski, Ekiel-Jezewska et al. 2009) to be:

$$v^* = \frac{v_c}{u_0} = KN\epsilon + c = K\varphi\epsilon^{-2} + c \qquad\qquad 4.1$$

Where $K = 6/5$ and $c = 1$. It is expected that as the volume fraction and N go to zero (isolated

particle) the velocity approaches the terminal speed and as the volume fraction and discretization

increase, the collective identity of the blob becomes more important than the behavior of each

individual particle. The velocity of the particle cloud, v_c is normalized by the terminal settling

velocity u_0 to give a non-dimensional settling speed v^*. In order to verify the code, simulations

were run at $Re_c < 0.01$; $Re_p \approx 0.000\ 075$ and $St = 0.000\ 157$. Other conditions of the

simulations were $\rho_p/\rho = 2.1$. The volume fraction of the simulations being ≤ 0.1 permitted us to

use the DPM simulations without the inter-particle collision forces. At low volume fractions we

can model the drag on each individual particle using the spherical drag law where the volume

fraction of the dispersed phase does not contribute to the interphase momentum exchange

parameter (Mindlin and Deresiewicz 1953). The value of the constant, K, in equation 4.1 is

closely matched in the simulations.

Table 4.1: Comparison of $N\epsilon$ dependence of settling speed in theory and simulations

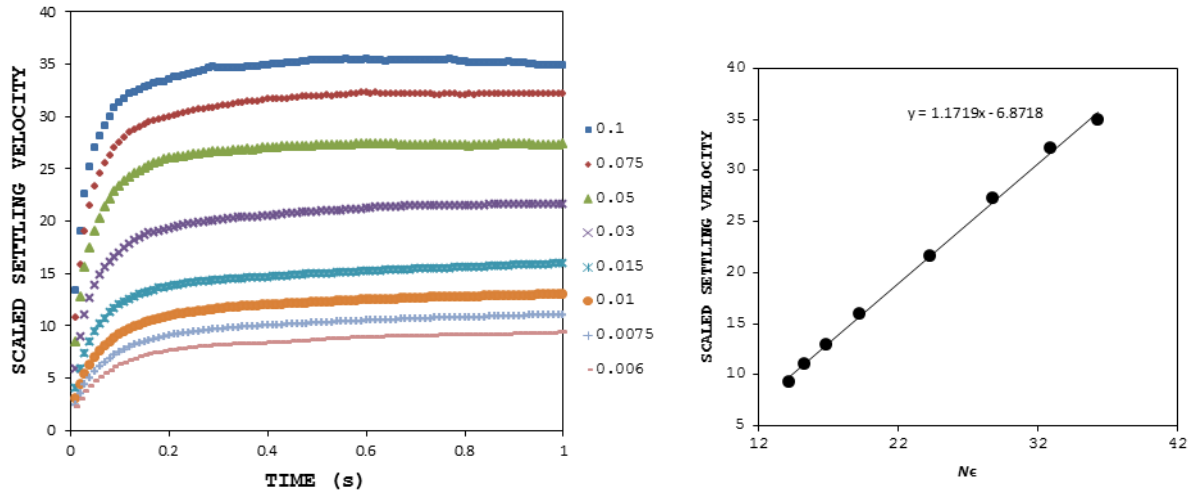|	K
Theory	1.2
Simulation	1.17

Figure 4.1: a.) Settling Velocity dependence on volume fraction; b.) Steady state settling velocity vs. $N\epsilon$

The fluctuating velocity, v' of each particle in a suspension which is the velocity around the mean settling speed was found to also be directly related to the volume fraction of the cloud. It is known that for homogenous suspensions that the amplitude of the fluctuations goes as the characteristic particle spacing, $\varphi^{1/3}$. We document the velocity fluctuations for a range of volume fractions on a logarithmic plot. The gradient of the line is found to be 0.3304 with an R^2 value of 0.9989 which confirms that the vertical velocity fluctuations are directly proportional to $\varphi^{1/3}$. The amplitude of the steady state horizontal velocity fluctuations is also dependent on the volume fraction in a similar fashion with a gradient of 0.3432 and an R^2 value of 0.9913.
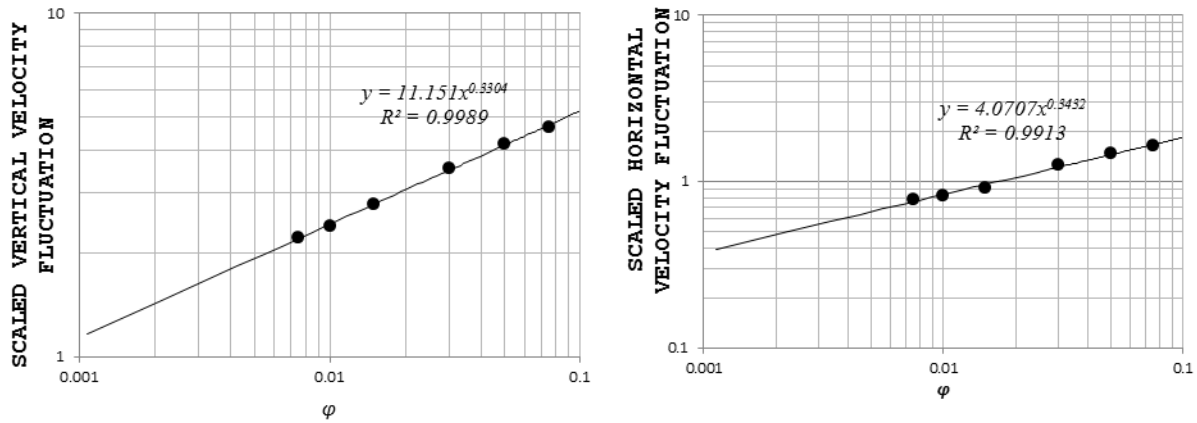
Figure 4.2: a.) Vertical Velocity fluctuations with volume fraction; b.) Horizontal velocity fluctuations with volume fraction

The fluctuating velocity is scaled by the terminal settling velocity of a particle in the fluid. We can relate $v'^*_{y\infty}$ to φ by the following relation $v'^*_{i\infty} = k_i \varphi^{1/3}$. The degree of anisotropy in the x and y axes can be compared by comparing the ratio of the pre-exponential. k_y (=11.151) is found to be almost 3 times the value of k_x (=4.0707) indicating strong anisotropy even for a geometrically symmetric entity like a spherical blob. There was no need to compare the fluctuations in the z-direction because a domain with a square cross-section was used and it will essentially be the same as the amplitude of the fluctuation in x-direction.

4.1.2 High Volume Fraction Simulations

Attempt has been made in literature to match Oseenlet simulations to experiments at conditions where the volume fraction of solids is close to 0.5 (Pignatel, Nicolas et al. 2011). The fundamental problem in using this approach is that at high volume fractions, the inter-particle effects can no-longer be ignored and the effect of the finite size of the particles and inertia must also be incorporated into the fluid flow equations. In these cases we utilized the dense particulate

flow in-house code using drag laws that incorporate the effect of the volume fraction and soft
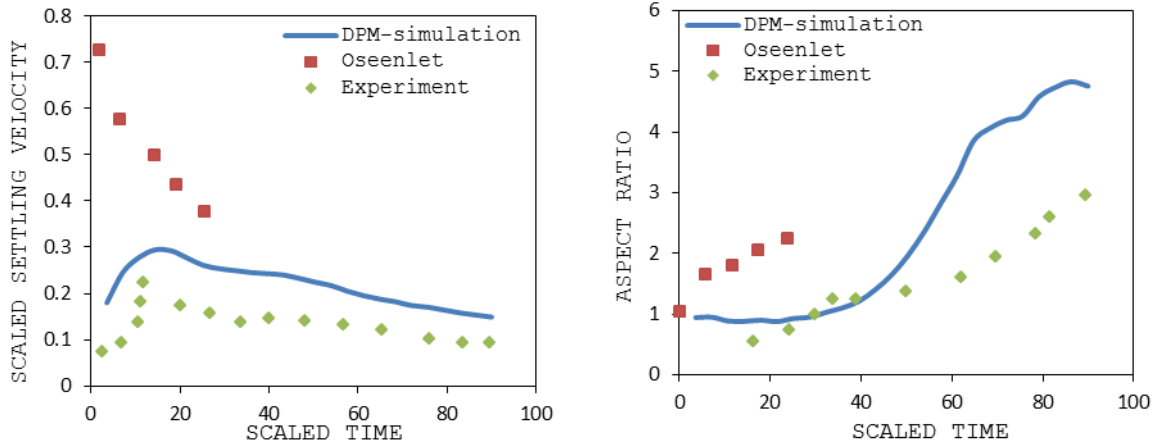
sphere inter-particle collision effects:

Figure 4.3: a.) Evolution of Scaled cloud settling velocity with scaled time at $Re_c = 11.4$ b.) Evolution of Cloud aspect ratio with scaled time at $Re_c = 11.4$
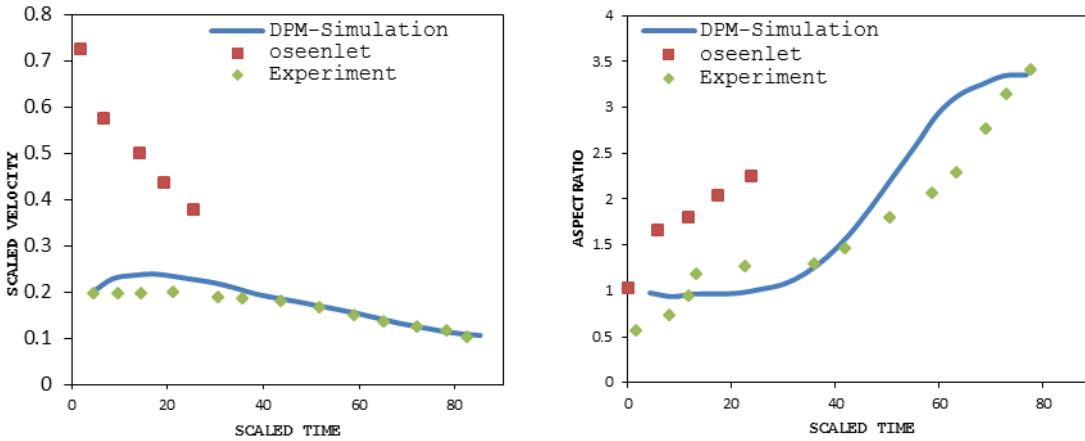

Figure 4.4 a.) Evolution of Scaled cloud settling velocity with scaled time at $Re_c = 14$ b.) Evolution of Scaled cloud aspect ratio with scaled time at $Re_c = 14$

As would be expected in the physical process, the cloud responds to gravity by accelerating from

zero but due to its horizontal expansion begins to decelerate after reaching a peak velocity.

The DPM simulations used in the work clearly out-performs the Oseenlet simulations used in

Pignatel, Nicolas et al. (2011). There are three key reasons for this. First, at the high volume

46

fraction (~0.5) conditions of the simulations and experiment, the drag on the individual particle can no longer be modelled with the straightfoward treatment of the stokeslet. The collective motion is stronger due to the slowly decaying $O(1/r)$ interparticle hydrodynamic interactions. Second, the size effects are not accounted for in the stokeslet simulations where the effect of volume fraction is completely ignored. Third, and also as a consequence of the high volume fraction and moderately high Re (~10-14), it is possible that short-range interparticle forces namely the collision dynamics may become significant. Oseenlets do not account for these. However at long time the oseenlet approaches experiments as particle become dispersed and the drag on the particles in the experiment become similar to that of an isolated particle. One may observe that the aspect ratio of the DPM simlulations does not grow as fast as that of the Oseenlet despite the fact that the non-linear inertia term is included in the governing equation. There is a brief period between the intialization of the flow and when the blob attains a maximum velocity which is not captured by Oseenlet simulations. The blob accelerates as a spherical entity in this regime as shown by the simulations but its aspect ratio begins to increase. This casuses a greater amount of drag to be experienced by the blob and it consequently begins to slow down.

4.1.3   Interaction among Multiple Drops

Further verification of the model is provided by exploring the interaction of two spherical particle clouds in comparison to the behaviour of two liquid drops qualitatively. If the discretization of the suspension cloud is fine enough, similarity in behaviour between suspension drops and immiscible liquid drops can be established (Machu, Meile et al. 2001). The behaviour of two particle clouds (or liquid drops) in an axisymmetric configuration is to create a pressure field around both drops that causes the leading drop to expand in the horizontal direction and

become oblate while the trailing drop expands in the vertical direction and becomes prolate.

Figure 4.7 shows the pressure field around a spherical particle configuration where only particles in the meridien plane are shown for clarity. The volume fraction, $\varphi = 0.075$, $\mu=0.1Pa\text{-}s$, $\rho=1200kgm^{-3}$.
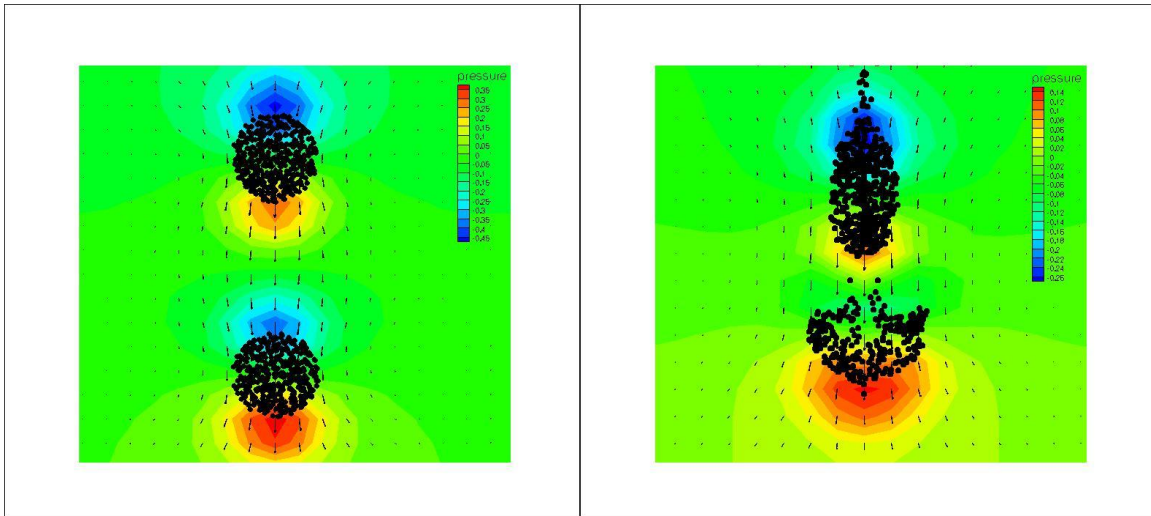

Figure 4.5: Pressure and velocity field around two trailing clouds at a.) t = 0.1 and b.) t=2.0s

The reason for this re-arrangement is that a high pressure stagnation point is setup at the leading end of the both clouds and a low pressure region at the rear. The low pressure region of the leading cloud creates a natural suction for the trailing cloud and deforms it accordingly. The consequence of the rearrangement of particles is an acceleration of the trailing cloud where it pokes through the slower leading particle cloud of the same radius. Leakage results in the trailing particle cloud because as the cloud becomes more prolate, it displays a greater tendency to loose particles in a tail (Machu, Meile et al. 2001).

Two clouds with dissimilar radius also show the same behaviour as two corresponding liquid drops with the leading smaller drop having a tendency to move slower than the trailing larger drop and to "coat" the surface of the trailing drop.
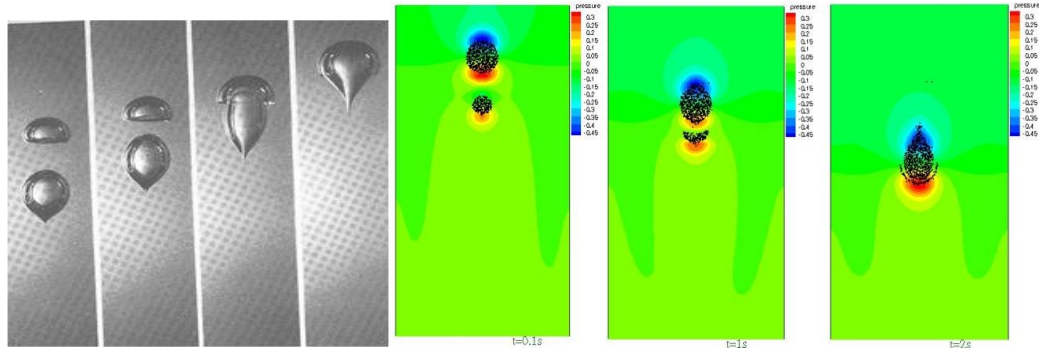
Figure 4.6: A comparison between two trailing bouyant drops of different radiuses and two trailing particle clouds of different radiuses in coaxial positions

Particle Cloud interactions in off-symmetric positions are also captured. The stagnation point at the leading edge of the trailing cloud and the low pressure region at the tail end of the leading cloud creates a natural suction for the distortion of both clouds.
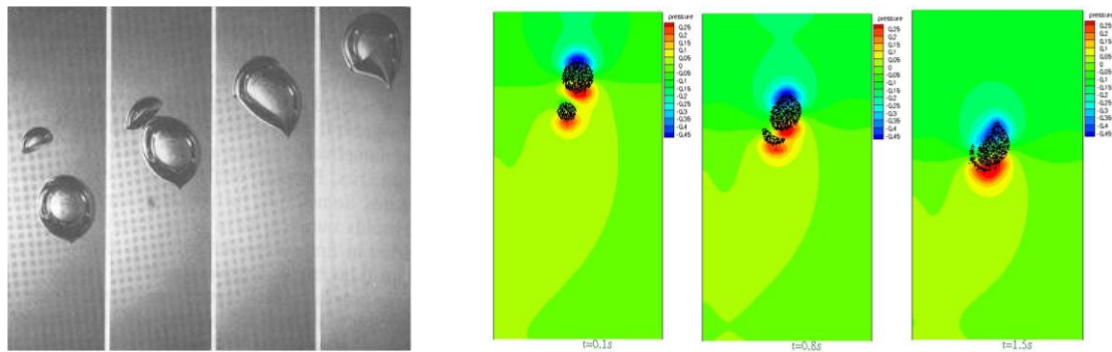

Figure 4.7: A comparison between two trailing drops of different radiuses and two trailing particle clouds of different radiuses in off-symmetry positions
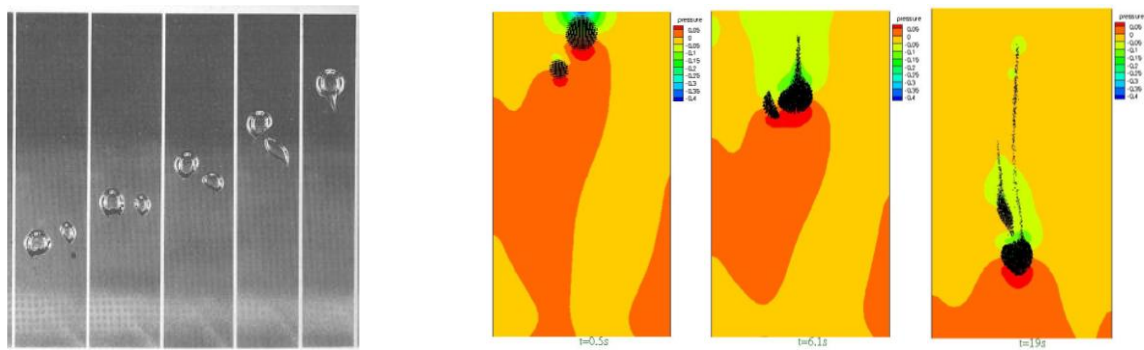

Figure 4.8: A comparison between two trailing drops of different radiuses and two trailing particle clouds of different radiuses in exaggerated off-symmetry positions

49

4.2   Particle Leakage At low Re_c

A spherical dispersion of particles settling under gravity will produce a well-defined tail of particles if the Reynolds number is sufficiently low (Nitsche and Batchelor 1997). Because of the randomness of the leakage process, the process of cloud settling can be termed an irreversible process. For the flow to be considered within the Stokes regime, the criterion used is based on the more stringent Re_c as opposed to the particle based Re_p. The random crossing of the imaginary boundary of the blob due to the many-body hydrodynamic interactions allows for such particles to be caught in the background fluid streamlines, swept to the back of the cloud and subsequently lost from the bulk of the cloud. Figure 4.11 shows the streamlines of the fluid flow field at a meridian plane that cuts through the center of the particle distribution..
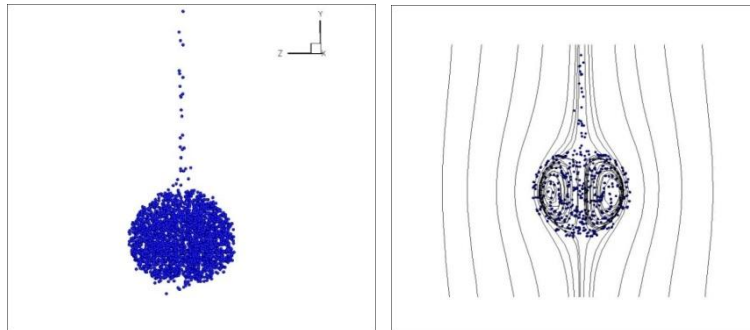

Figure 4.9: Particle leakage at low Reynolds number

Because inertia is almost non-existent in this regime, the particles can no longer catch-up with the rest of the cloud and are lost in an axial tail behind the blob. The streamlines are obtained by plotting the velocity field in a frame of reference that is moving with the settling cloud velocity.

We define a leaked particle as one that fulfills the criterion $\left|y_p - \bar{y}\right| > 1.2R$. The cutoff is greater than the actual radius of the cloud so as to allow for the negligible deviations from the roughly spherical shape of the cloud.

4.2.1 Rate of Particle Leakage and Initial Particle number

Since particle leakage is a function of the long-range inter-particle interactions, and hence a statistically random process that depends on the configuration and number of particles, we can assume that the rate of particle leakage should be $f(N_p)$. We studied the leakage of particles with respect to initial particle number. Particles in the simulation are mono-size with $d_p = 120\mu$m. Conditions for the simulations performed are given in Table 4.2.

Table 4.2: Parameters for the Particle number parameter study

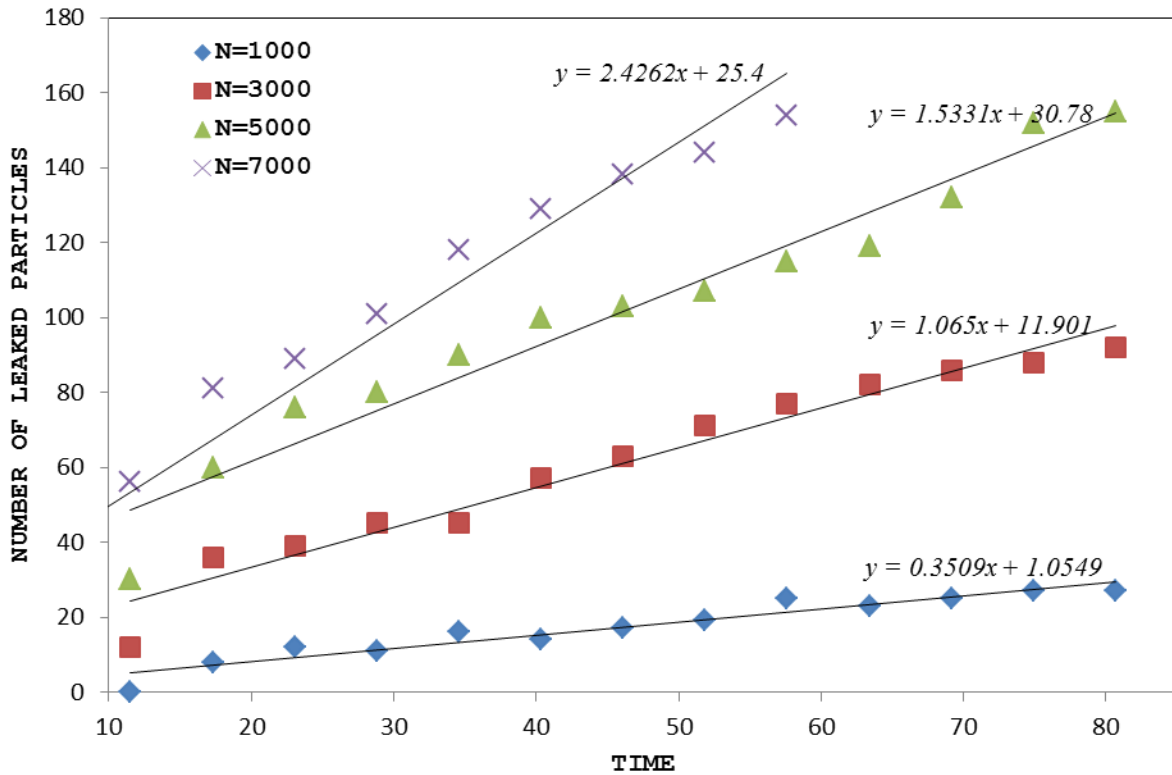| N_p	1000	3000	5000	7000
Re_p	0.000 300 67	0.000 300 67	0.000 300 67	0.000 300 67
φ	0.023	0.023	0.023	0.023

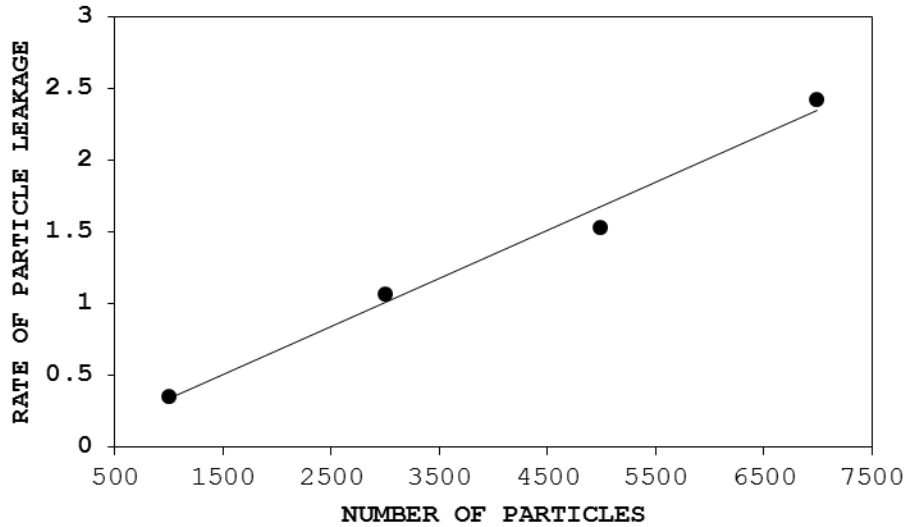Figure 4.10: Particle Leakage with time

Figure 4.11: Rate of Particle leakage with initial number of particles

4.3 Breakup At moderate Re_c

There is a qualitative similarity between the breakup-pattern of particle clouds simulated in this work at moderate Reynolds number. The simulation conditions are: $Re_c = 5.0$, $\rho_p/\rho = 2.1$, $St = 0.005266$. Figure 4.14 shows that the DPM simulation is adequate to capture the breakup of the blob into two secondary blobs.
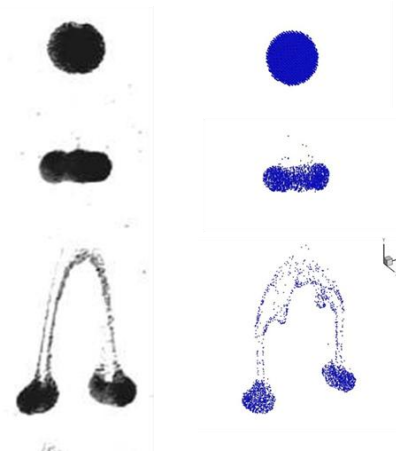

Figure 4.12: Comparison between breakup into two secondary drops in experiments (left) and simulation (right) at $Re_c \approx 5.0$

4.3.1   Effect of Domain Shape on Cloud Breakup

In the simulations carried out, the domain had a square cross-section. For the simulations performed in the Reynolds number parametric study (see section 4.3.3), four secondary blobs were produced with consistency indicating that the number of secondary drops produced seems to depend more on the shape of the boundaries than on the Reynolds number of the system. This is slightly different from the findings of Bosse, Kleiser et al. (2005) who were able to produce different breakup patterns by varying the grid coarseness and the Reynolds number using periodic boundaries for all their simulations. An investigation was also made into the effect of the nature of the boundary conditions and no change in the fundamental pattern of breakup was observed. This is in agreement with the observations outlined by Bosse, Kleiser et al. (2005). Three boundary configurations were used – the bounded box, fully periodic boundaries, and no-slip boundary conditions in the manner of (Nguyen and Ladd 2005). The bounded box uses periodic boundaries for the vertical walls, fully periodic uses periodic boundaries for all the walls.

Because of the strong dependence of the number of secondary blobs on the shape of the boundaries we can expect 2 secondary blobs to develop in say a rectangular cross-section. The shape of the domain used in the experiment has a rectangular cross-section and is thus the reason for the amplification of the mode that leads to 2 blobs. This is reproduced in the simulations. We show in other simulations (Figure 4.15) that the number of blobs could be up to 4 where the domain has a square cross section and as many to 6 in the case of a circular domain and all blobs have the same initial conserved quantities. It is concluded that the secondary drops produced are independent of whether the boundaries are impenetrable walls or periodic, what matters is the shape of the boundaries.

We also see that there is no quantitative difference when the domain cross-section used is a square irrespective of the nature of the boundaries by comparing the velocity fluctuations and the aspect ratio evolution for the three types of boundaries. This result has previously been reported for homogeneous sedimentation (Nguyen and Ladd 2005).

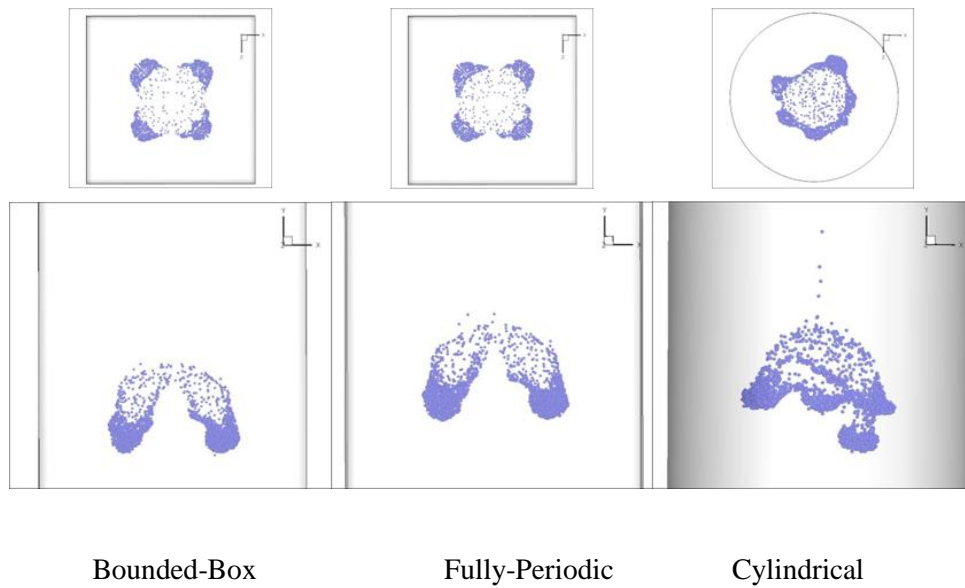Bounded-Box   Fully-Periodic   Cylindrical

Figure 4.13: Effect of nature of and shape of boundary on breakup pattern showing top view (top) and side view (bottom)
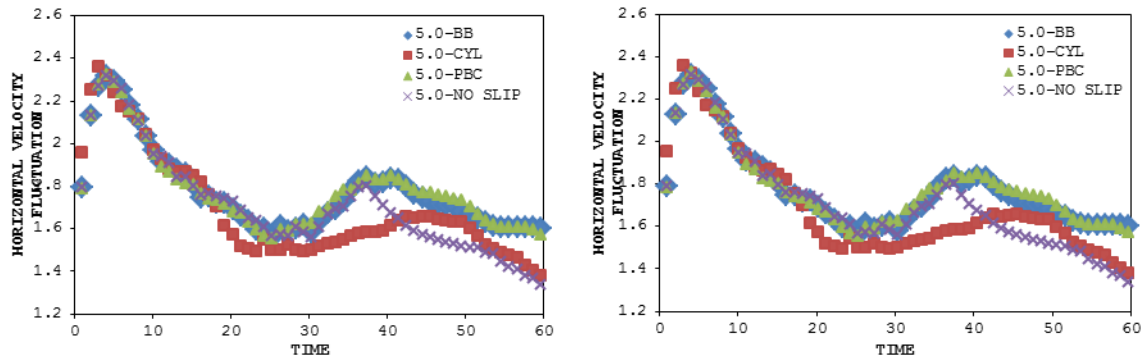

Figure 4.14: Effect of Nature of boundaries on velocity fluctuations in a.) Vertical and b.) horizontal directions.

4.3.2 Effect of Initial Particle Distribution on Breakup

There is no evidence to indicate that the initial particle distribution has a significant role to play in the secondary breakup pattern. The evolution for an initially random configuration of particles is the same as a regularly spaced distribution of particles. A random number generator was employed to give an initially random particle distribution of the cloud of particles. $Re_c = 5.0$, Re_p =0.00186 , $St = 0.0017$, and $\rho_p/\rho = 2.1$ where the initial volume fraction in both simulations was $\varphi = 0.023$. Simulations showed a bias to the shape of the boundary than the initial distribution of the particles. The breakup of the cloud produces 2 secondary clouds in keeping with the rectangular cross-section of the domain. This breakup pattern is the same as that produced when the initial particle distribution was a regular square lattice clipped off at the corners to give an initially spherical distribution.
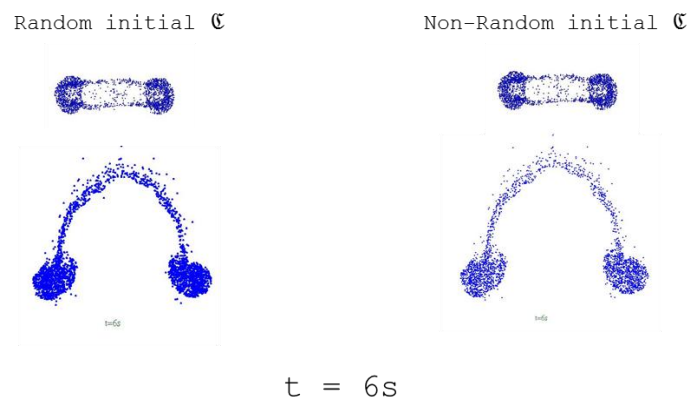

Figure 4.15: Breakup pattern for a.) An initially random b.) Non-random particle distribution

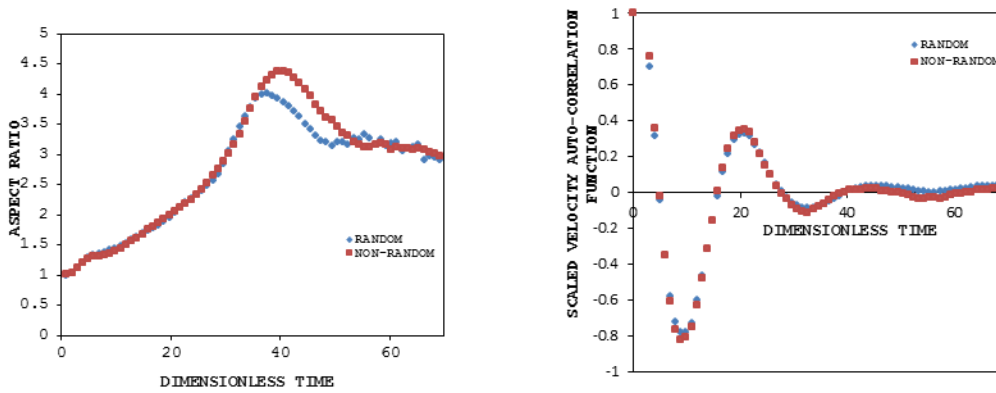We also make a quantitative comparison of both cases.

Figure 4.16: Comparison of Cloud Evolution for initially random and non-random particle distributions a.) Aspect ratio evolution; b.) Velocity auto-correlation function evolution

Table 4.3: Comparison of break up quantities of and initially random cloud configuration and non-random configuration of particles

	RANDOM INITIAL DISTRIBUTION	NON-RANDOM INITIAL DISTRIBUTION
t_b(s)	3.8	3.9
l_b(m)	0.053831	0.054415
γ_c	4.01	4.306

It is observed from the results that there is no quantitative or qualitative proof that the randomness of the initial distribution has anything to do with the breakup characteristic of the blob with both having very similar breakup patterns and characteristics. The breakup pattern is thus more a function of the large-scale, hydrodynamic interactions with the boundary and the shape of these boundaries than the isolated individual positions of the particles.

4.3.3 Reynolds Number Studies, Cloud evolution and Breakup

We can quantify the life of the cloud by the break-up time and break-up length. The time between the release of the cloud from rest and the breakup of the cloud into secondary blobs is here defined as the breakup time and the distance travelled is the breakup length which is closely

associated with t_b. Quantitatively, we define this point as when the aspect ratio of the cloud peaks and then begins to fall as a result of the steady loss of symmetry.

The aspect ratio of the cloud denoted as γ is an important shape characteristic because it quantifies the ratio between the degree of oblation and the degree of prolation. This value affects the effective projected area in the direction of motion of the cloud and directly affects the effective drag seen by the swarm. We calculate this value as square root of the variance of the particle displacement in the x-direction to the value in the y-direction. In order to utilize a more robust form of this statistic, the particles that are deemed to have leaked from the blob i.e. particles that are a distance $>1.20R_c$ are not included in the calculation which would otherwise be sensitive to outliers. By defining γ in this way we avoid the arbitrariness of measuring the cloud dimensions based on the furthest particles in each direction.

$$\gamma = \frac{\sqrt{\sum_{i=1}^{K} f_i \cdot (x_i - \bar{x})^2}}{\sqrt{\sum_{i=1}^{K} g_i \cdot (y_i - \bar{y})^2}} \qquad 4.2$$

Pignatel, Nicolas et al. (2011) mention that the breakup time is a quantity dependent on only the number of particles in the simulation. It was observed in our simulations that the breakup time and length bear a relationship to Re_c.

Figure 4.17 shows how the aspect ratio changes with time for different Reynolds numbers. There is a rapid increase in the aspect ratio at higher Reynolds numbers and the chart is truncated at the moment of break-up where a description of the aspect ratio using equation becomes meaningless. When $Re_c \ll 1$, the cloud maintains a robust spherical axisymmetric structure and the shape remains a closed spherical cluster.
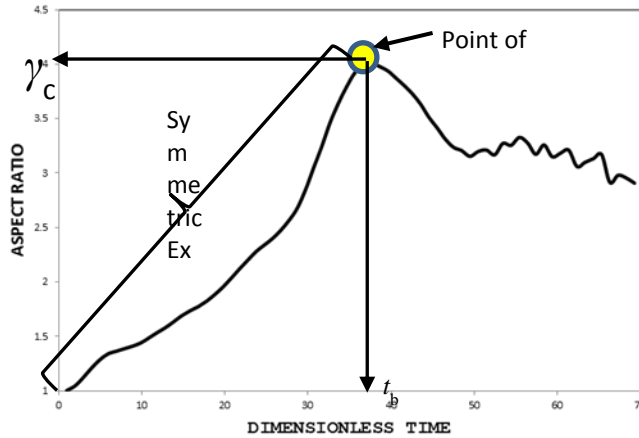
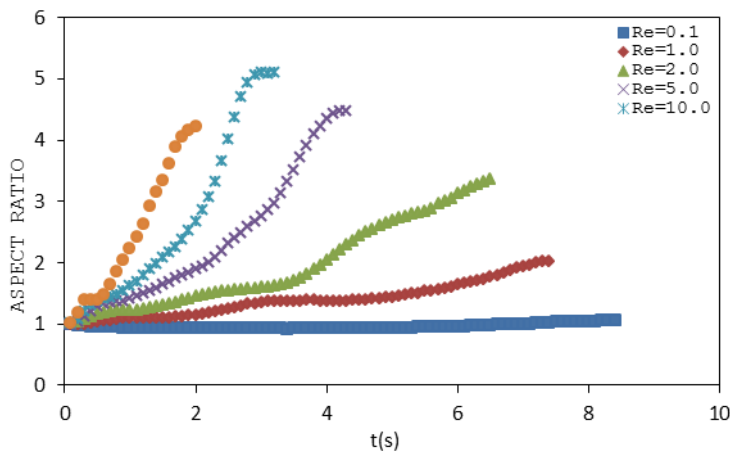Figure 4.17: Schematic showing the evolution of the cloud aspect ratio before and after the point of breakup.

Figure 4.18: Aspect Ratio evolution with time at different Reynolds number

In order for breakup to occur, a critical aspect ratio γ_c must be reached. At this point, the cloud has expanded in the lateral direction into a symmetric, open torus and the higher density cloud forces through the lower density fluid against the stabilizing effect of viscosity. Figure 4.19 shows the point at which this occurs. In the simulations performed we observe that γ_c is

independent of the Reynolds number of the flow and this is so because of the uncertainty that

sets in as the flow becomes more chaotic.

Table 4.4: Critical aspect ratio just prior to breakup

Re_c	γ_c
2	3.624912
5	4.478809
10	5.099754
20	5.062558
30	4.370129
40	4.62275
50	4.214646

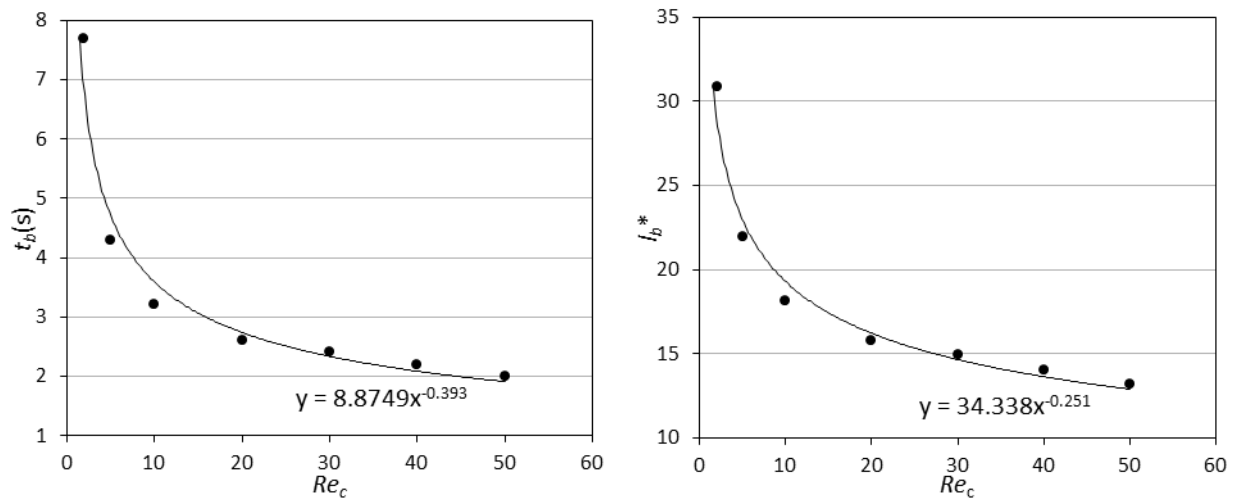We plot the breakup time and length respectively against Re_c and find a relationship between

both:

Figure 4.19: Effect of Rec on a.) The breakup time; b.) breakup length

From figure 4.19, the breakup time increases asymptotically to ∞ as the Reynolds number goes

to zero to obtain the following scaling law: $t_b = 8.8749Re_c^{-0.393}$. Also, the non-dimensional

breakup length, which is the length travelled by the cloud scaled by the initial radius of the cloud

is observed to decrease with Reynolds number and the scaling law obtained

is $l_b = 34.338 Re_c^{-0.251}$. This later result at first seems counter-intuitive because at higher Re_c,

we would expect that the blob would travel a longer distance in a short time and thus the breakup

length should be longer. However, if we consider that the dispersion of the cloud in the lateral

direction means that the effective drag on the cloud increases as it expands and thus reduces the

velocity of the cloud. We can observe this by quantifying the expansion of the cloud using the

aspect ratio.

4.3.4 Velocity Fluctuation Auto-correlation

One measure of characterizing the evolution of the cloud is to look at the behavior of the VACF

with time. This function mathematically correlates the individual velocity fluctuations of the

particles with the velocity fluctuation at the beginning of the clouds descent and physically tells

us about the hydrodynamic interactions between the particles as they collectively travel in the

fluid and the degree of irreversibility of the system. For a fully reversible process in which the

viscous dissipation term fully dampens out any distorting effects of inertia on the blob, the

velocity correlation should follow a non-decaying, sinusoidal wave in keeping with the Hill's

vortices generated within the cloud substructure. In order to get meaningful results for the

velocity auto-correlation function, the suspension cloud should be allowed to reach some steady

state. The velocity fluctuations subsequently are then benchmarked against this "steady state".

This places a constraint on the minimum length of the domain. Computational time scales

directly as the computational cell count and by extension the computation volume. Simulations

of liquid-solid systems have been known to be on the order of one month using other approaches

like Lattice Boltzmann simulations (Nguyen and Ladd 2005). If the mean particle velocity in a

given suspension is given as $\bar{v}_p = \frac{1}{N_p}\sum_{k=1}^{N_p} v_{p,k}$ time-dependent fluctuation of the particle

velocity from this mean $v'_{p,k} = v_{p,k} - \bar{v}_p$. We can now define the velocity auto-correlation

function, *VACF* as

$$VACF = \frac{1}{N_P}\sum_{k=1}^{N_P} v'_k(t_0)v'_k(t)$$

4.3

In order to study the sensitivity of the evolution pattern of the sedimenting cloud, we observe

how the following characteristics change with time: the aspect ratio, the velocity fluctuations and

the velocity auto-correlation function of any given system. The key physical property used in

changing the Reynolds number was the dynamic viscosity. The initial volume

fraction $\varphi = 0.023$ and the density ratio $\rho_p/\rho = 2.1$ were kept constant in all simulations. The

simulation domain used had a square cross-section with a dimension of $W/2R_c = 21.806$ with

131,072 hexahedral mesh elements. Boundary conditions used were the impenetrable wall

boundary for all six faces of the domain.

Figure 4.20 shows the evolution of the dimensionless average settling velocity for different

Reynolds numbers. The three stages of rapid acceleration, self-preservation and dispersion are

noticeable in the higher Reynolds numbers. At lower Re_c, the acceleration phase and self-

preservation phase are longer with Rec = 0.1 showing the highest tendency for self-preservation.

This is more noticeable when the velocity auto-correlation function is observed (Figures 4.21 &
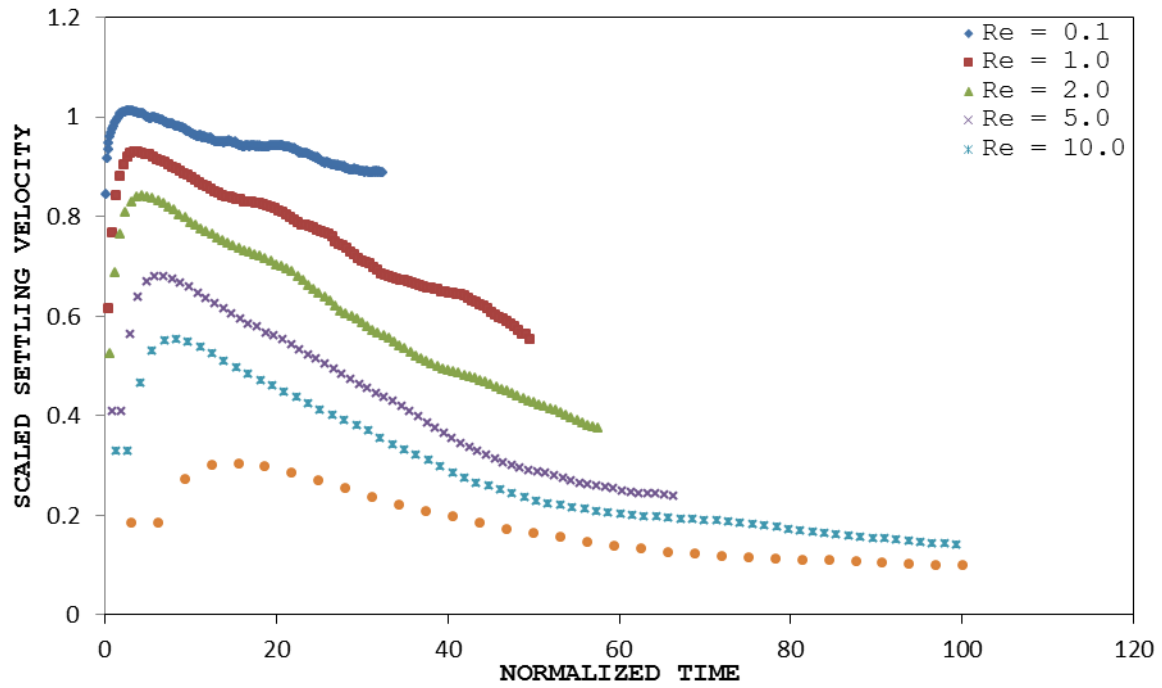
4.22).

Figure 4.20: Normalized Average settling velocity of Cloud vs. normalized time for different Reynolds numbers
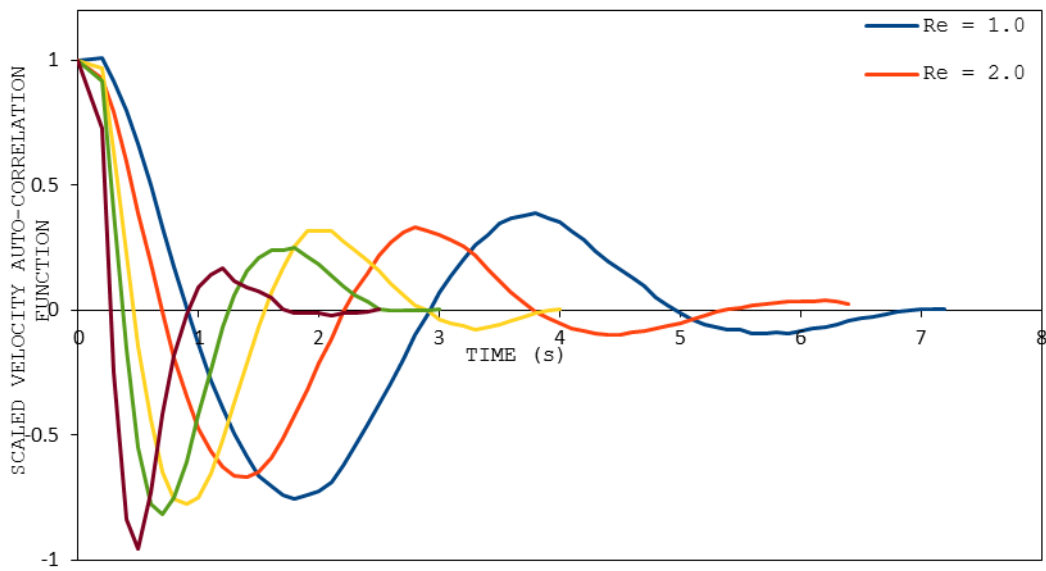

Figure 4.21: Scaled Velocity Auto-correlation Function with time at different Reynolds Numbers
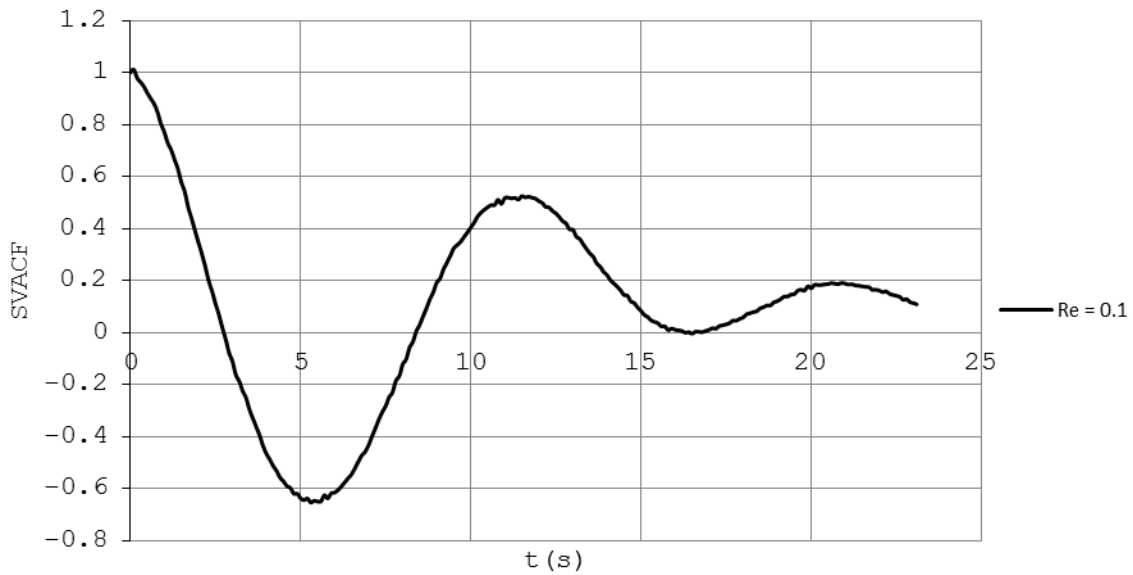
Figure 4.22: Velocity Auto-correlation function at $Re_c = 0.1$

4.3.5 The evolution of the cloud

We present some results for the parameter study we conducted and show that at lower Reynolds numbers, the axisymmetric nature of the cloud is preserved (See Figures 4.23 – 4.25). At moderate to high Re_c, the non-linearity of the inertia term becomes dominant and the blob quickly loses its symmetry and breaks up (See Figures 4.26-4.28).
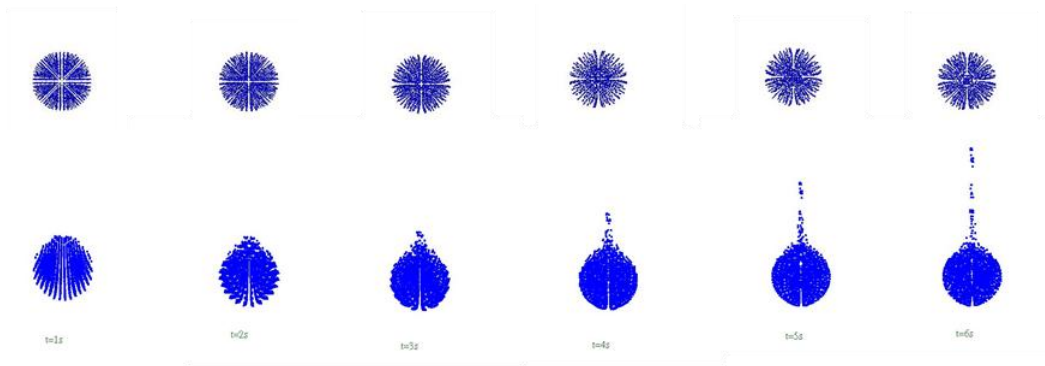

Figure 4.23: Shape evolution at $Re_c = 0.1$

Figure 4.24: Shape evolution at $Re_c = 1.0$

Figure 4.25: Shape evolution at $Re_c = 2.0$

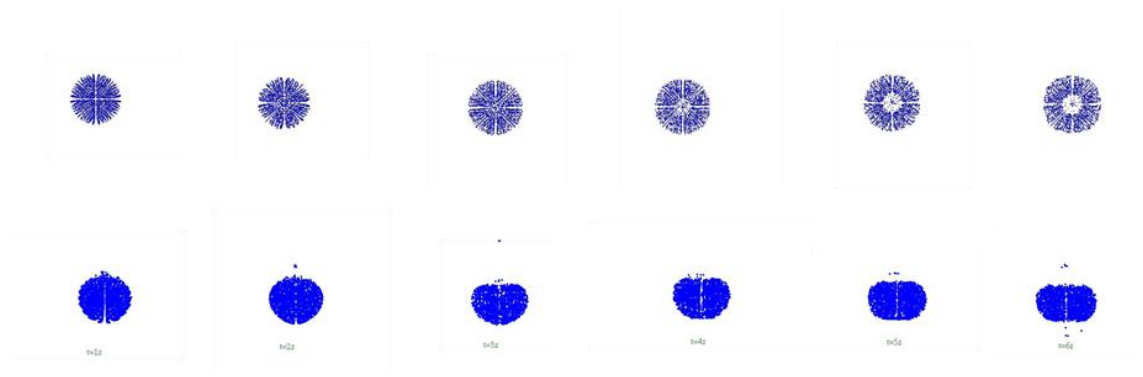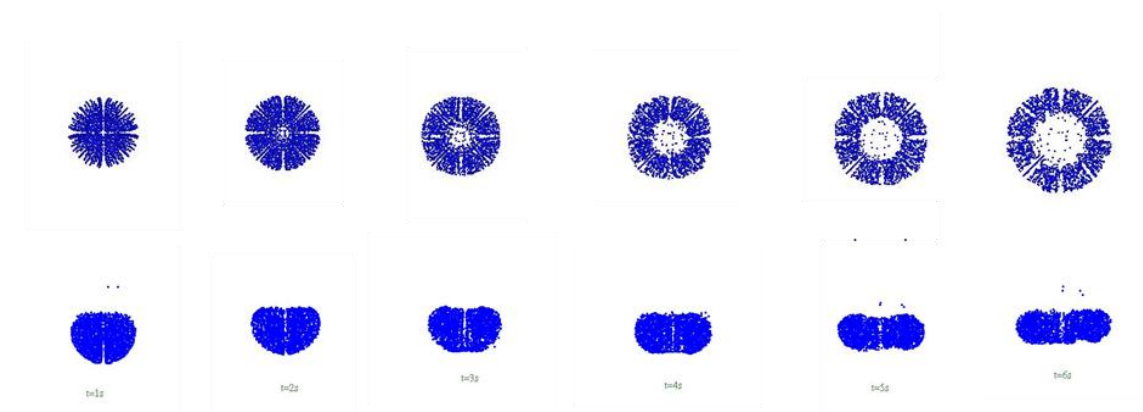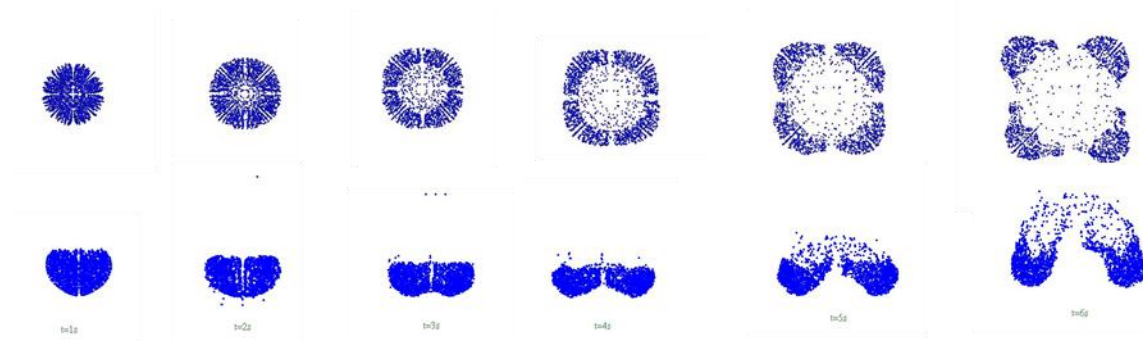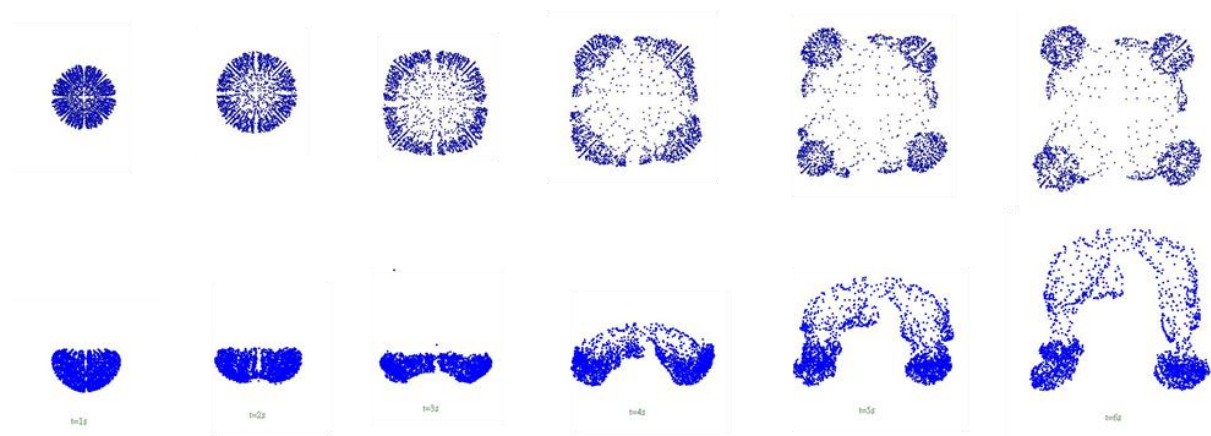Figure 4.26: Shape evolution at $Re_c = 5.0$
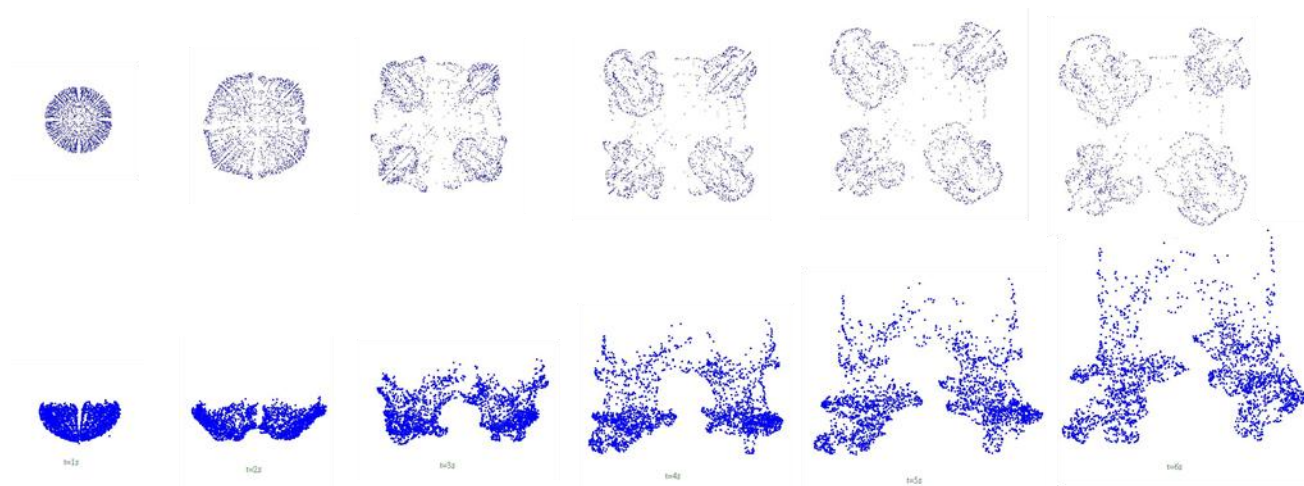
Figure 4.27: Shape evolution at $Re_c = 10.0$

Figure 4.28: Shape evolution at $Re_c = 50.0$

Figures 4.26 – 4.28 are the shape evolution when Re_c is moderate. The evolution shows that the

mode of dispersion into the host fluid is to go through hydrodynamic instability that causes a loss

of symmetry, secondary blob formation and subsequently dispersion.

5.0   Conclusions

The sedimentation of a cloud of particles in a viscous fluid at low and moderate Reynolds numbers has been studied. We looked at the volume fraction dependence of the settling cloud and find a similar dependence in the simulations as in the theoretical predictions of (Nitsche and Batchelor 1997). The average cloud settling velocity and the velocity fluctuations around this average are found to have a linear dependence on $\varphi^{1/3}$ at negligible Reynolds number. The velocity fluctuations display strong anisotropy with the magnitude of the vertical component almost three times the magnitude of the horizontal component.

At high volume fractions, and moderate Reynolds numbers, particle-particle interactions become important and a drag law that accounts for the finite volume of particles is required in the modeling.

Similarities in the interaction between a system of two particle clouds and a system of two immiscible droplets was established with an observed increase in the velocity of the trailing cloud due to drag reduction in the wake of the leading cloud. The formation of the stagnation points at the leading front of the cloud is pointed to as the cause of shape deformation in these systems.

Particle leakage at low Reynolds number was established and found to be directly related to the initial number of particles

At higher Reynolds numbers, the cloud of particles evolved into an open torus and subsequently loses its axi-symmetry and breaks-up into a number of secondary clouds. This process is a type of Rayleigh-Taylor instability and the number of secondary drops was found in our simulations to be dependent on the shape of the boundaries used rather than the nature of the boundaries.

Breakup at moderate Re_c is found to occur after a critical aspect ratio is reached and a scaling was proposed for dependence of the breakup length and breakup time on Re_c. It may be necessary in future works to find the dependence of the critical aspect ratio on the number of particles in the particle cloud.

References

Abade, G. C. and F. R. Cunha (2007). "Computer simulation of particle aggregates during sedimentation." Computer Methods in Applied Mechanics and Engineering **196**(45–48): 4597-4612.

Alabrudzinski, S., M. L. Ekiel-Jezewska, et al. (2009). "Particle clusters settling under gravity in a viscous fluid." Physics of Fluids **21**(7): 073302.

Batchelor, G. K. (1972). "Sedimentation in a dilute dispersion of spheres." Journal of Fluid Mechanics **52**(02): 245-268.

Bosse, T., L. Kleiser, et al. (2005). "Numerical simulation of finite Reynolds number suspension drops settling under gravity." Physics of Fluids **17**(3): 037101.

Brady, J. F. and G. Bossis (1988). "Stokesian Dynamics." Annual Review of Fluid Mechanics **20**(1): 111-157.

Brenner, M. P. (1999). "Screening mechanisms in sedimentation." Physics of Fluids **11**(4): 754-772.

Caflisch, R. E. and J. H. C. Luke (1985). "Variance in the sedimentation speed of a suspension." Physics of Fluids **28**(3): 759-760.

Campbell, C. S. and C. E. Brennen (1985). "Computer simulation of granular shear flows." Journal of Fluid Mechanics **151**: 167-188.

Crowe, C. T. (2012). Multiphase flows with droplets and particles. Boca Raton, CRC Press.

Crowe, C. T., M. P. Sharma, et al. (1977). "The particle-source-in-cell (PSI-CELL) model for gas-droplet flow." Transactions of the ASME-Journal of Fluid Engineering **99**: 325-332.

Cundall, P. A. and O. D. L. Strack (1979). "Discrete Numerical-Model for Granular Assemblies." Geotechnique **29**(1): 47-65.

Davis, R. H. and A. Acrivos (1985). "Sedimentation of Noncolloidal Particles at Low Reynolds Numbers." Annual Review of Fluid Mechanics **17**(1): 91-118.

Deen, N. G., M. V. Annaland, et al. (2007). "Review of discrete particle modeling of fluidized beds." Chemical Engineering Science **62**(1-2): 28-44.

Ekiel-Jezewska, M. L., B. Metzger, et al. (2006). "Spherical cloud of point particles falling in a viscous fluid." Physics of Fluids **18**(3): 038104.

Ergun, S. (1952). "Fluid flow through packed columns." Chemical Engineering Progress **48**: 89-94.

Favier, J. F., M. H. Abbaspour-Fard, et al. (2001). "Modeling nonspherical particles using multisphere discrete elements." Continuous and Discontinuous Modelling of Cohesive-Frictional Materials **127**(October).

Gidaspow, D. (1994). "Multiphase Flow and Fluidization - Continuum and Kinetic Theory Descriptions." Academic Press, San Diego.

Glowinski, R., T. W. Pan, et al. (1999). "A distributed Lagrange multiplier/fictitious domain method for particulate flows." International Journal of Multiphase Flow **25**(5): 755-794.

Goldschmidt, M. J. V., R. Beetstra, et al. (2004). "Hydrodynamic modelling of dense gas-fluidised beds: comparison and validation of 3D discrete particle and continuum models." Powder Technology **142**(1): 23-47.

Guazzelli, E. and J. Hinch (2011). "Fluctuations and Instability in Sedimentation." Annual Review of Fluid Mechanics, Vol 43 **43**: 97-116.

Hoomans, B. P. B., J. A. M. Kuipers, et al. (1996). "Discrete particle simulation of bubble and slug formation in a two-dimensional gas-fluidised bed: A hard-sphere approach." Chemical Engineering Science **51**(1): 99-118.

Hu, H. H., D. D. Joseph, et al. (1992). "Direct simulation of fluid particle motions." Theoretical and Computational Fluid Dynamics **3**(5): 285-306.

Koch, D. L. and E. S. G. Shaqfeh (1991). "Screening in sedimenting suspensions." Journal of Fluid Mechanics **224**: 275-303.

Kohnen, G., M. Ruger, et al. (1994). Convergence Behaviour for Numerical Calculations by the Euler/Lagrange method for strongly coupled phases. ASME Fluids Engineering Divisioni Summer Meeting. C. T. Crowe, A. Johnson, A. Prosperetti, M. Sommerfeld and Y. Tsuji. Lake Tahoe, U.S.A., ASME-FED. **185:** 191-202.

Kohring, G. A., S. Melin, et al. (1995). "Computer simulations of critical, non-stationary granular flow through a hopper." Computer Methods in Applied Mechanics and Engineering **124**(3): 273-281.

Kuusela, E. (2005). Steady State Sedimentation of Non-Brownian Particles With Finite Reynolds Number, Helsinki University of Technology. **Ph.D.**

Ladd, A. and R. Verberg (2001). "Lattice-Boltzmann simulations of particle-fluid suspensions." Journal of Statistical Physics **104**(5-6): 1191-1251.

Machu, G., W. Meile, et al. (2001). "Coalescence, torus formation and breakup of sedimenting drops: experiments and computer simulations." Journal of Fluid Mechanics **447**: 299-336.

Metzger, B. and J. E. Butler (2012). "Clouds of particles in a periodic shear flow." Physics of Fluids **24**(2).

Metzger, B., M. Nicolas, et al. (2007). "Falling clouds of particles in viscous fluids." Journal of Fluid Mechanics **580**: 283-301.

Mindlin, R. D. and H. Deresiewicz (1953). "Elastic spheres in contact under varying oblique forces." Transactions of the ASME-Series E **20**: 327-344.

Motomiya, M. and T. Karino (1984). "Flow patterns in the human carotid artery bifurcation." Stroke **15**(1): 50-56.

Muthukumar, S. and R. DesRoches (2006). "A Hertz contact model with non-linear damping for pounding simulation." Earthquake Engineering & Structural Dynamics **35**(7): 811-828.

Mylyk, A., W. Meile, et al. (2011). "Break-up of suspension drops settling under gravity in a viscous fluid close to a vertical wall." Physics of Fluids **23**(6): 063302.

Nguyen, N.-Q. and A. J. C. Ladd (2005). "Sedimentation of hard-sphere suspensions at low Reynolds number." Journal of Fluid Mechanics **525**: 73-104.

Nicolai, H., B. Herzhaft, et al. (1995). "Particle velocity fluctuations and hydrodynamic self-diffusion of sedimenting non-Brownian spheres." Physics of Fluids **7**(1): 12-23.

Nitsche, J. M. and G. K. Batchelor (1997). "Break-up of a falling drop containing dispersed particles." Journal of Fluid Mechanics **340**: 161-175.

Pignatel, F., M. Nicolas, et al. (2011). "A falling cloud of particles at a small but finite Reynolds number." Journal of Fluid Mechanics **671**: 34-51.

Pyrak-Nolte, L. J. and M. K. Olander "PARTICLE SWARMS IN SMOOTH-WALLED FRACTURES."

Rahimipour, H. and D. Wilkinson (1992). Dynamic Behaviour of Particle Clouds. 11th Australasian Fluid Mechanics Conference. University of Tasmania, Hobart, Australia.

Rhie, C. M. and W. L. Chow (1983). "Numerical study of the turbulent flow past an airfoil with trailing edge separation." AIAA Journal **21**: 1525-1532.

Richardson, J. F. and W. N. Zaki (1954). "Sedimentation and Fluidization." Trans. Inst., Chem. Eng., **32**: 35-53.

Rowe, P. N. and G. A. Henwood (1961). "Drag Forces in a Hydraulic Model of a Fluidized Bed - Part-1." Trans. Inst., Chem. Eng., **39**: 43.

Rubinstein, J. and S. Torquato (1989). "Flow in random porous media: mathematical formulation, variational principles, and rigorous bounds." Journal of Fluid Mechanics **206**: 25-46.

Sangani, A. S. (1987). "Sedimentation in ordered emulsions of drops at low Reynolds numbers." Zeitschrift für Angewandte Mathematik und Physik (ZAMP) **38**(4): 542-556.

Sangani, A. S. and A. Acrivos (1982). "Slow flow through a periodic array of spheres." International Journal of Multiphase Flow **8**(4): 343-360.

Segre, P. N., E. Herbolzheimer, et al. (1997). "Long-range correlations in sedimentation." Physical Review Letters **79**(13): 2574-2577.

Swan, J. W. and J. F. Brady (2011). "The hydrodynamics of confined dispersions." Journal of Fluid Mechanics **687**: 254-299.

Tsuji, Y., T. Kawaguchi, et al. (1993). "Discrete particle simulation of two-dimensional fluidized bed." Powder Technology **77**(1): 79-87.

Van der Hoef, M. A., M. Ye, et al. (2006). "Multi-scale modeling of gas-fluidized beds." Advances in Chemical Engineering **31**: 65.

Veeramani, C., P. D. Minev, et al. (2007). "A fictitious domain formulation for flows with rigid particles: A non-Lagrange multiplier version." Journal of Computational Physics **224**(2): 867-879.

Wen, Y. C. Y., Y.H., (1966). "Mechanics of Fluidization." Chemical Engineering Progress Symposium Series **62**: 100-111.

Wu, C. L., A. S. Berrouk, et al. (2009). "Three-dimensional discrete particle model for gas–solid fluidized beds on unstructured mesh." Chemical Engineering Journal **152**(2–3): 514-529.

Wu, C. L., K. Nandakumar, et al. (2011). "Enforcing mass conservation in DPM-CFD models of dense particulate flows." Chemical Engineering Journal **174**(1): 475-481.

Appendix A: Letter of Permission

Figure 2.1: Three regimes of cloud settling based on particle and cloud scale inertia is reproduced with permission from material published in Pignatel, F., M. Nicolas, et al. (2011). "A falling cloud of particles at a small but finite Reynolds number." <u>Journal of Fluid Mechanics</u> **671**: 34-51. The scanned letter of approval is given:

CAMBRIDGE UNIVERSITY PRESS LICENSE
TERMS AND CONDITIONS

Jul 02, 2013

This is a License Agreement between Oladapo Ayeni ("You") and Cambridge University Press ("Cambridge University Press") provided by Copyright Clearance Center ("CCC"). The license consists of your order details, the terms and conditions provided by Cambridge University Press, and the payment terms and conditions.

All payments must be made in full to CCC. For payment instructions, please see information listed at the bottom of this form.

License Number	3181030586932
License date	Jul 02, 2013
Licensed content publisher	Cambridge University Press
Licensed content publication	The Journal of Fluid Mechanics
Licensed content title	A falling cloud of particles at a small but finite Reynolds number
Licensed content author	FLORENT PIGNATEL, MAXIME NICOLAS and ÉLISABETH GUAZZELLI
Licensed content date	Mar 25, 2011
Volume number	671
Issue number	-1
Start page	34
End page	51
Type of Use	Dissertation/Thesis
Requestor type	Author
Portion	Text extract
Number of pages requested	1
Author of this Cambridge University Press article	No
Author / editor of the new work	Yes
Order reference number	
Territory for reuse	World
Title of your thesis / dissertation	Sedimentation of Swarms of Particles at Low and Moderate Reynolds Numbers
Expected completion date	Jul 2013
Estimated size(pages)	75
Billing Type	Invoice
Billing address	110 South Stadium Road
	Chemical Engineering

Vita

Oladapo Ayeni was born in Lagos, Nigeria, to Oladapo and Modupeola Ayeni. After graduating from secondary school at King's College, Lagos in 2000, he went on to study Chemical Engineering at the University of Lagos, Akoka, Lagos, Nigeria, earning a Bachelor of Science degree in 2006. Oladapo has some experience working in the financial industry having worked at Zenithbank Plc, Nigeria between September 2008 and December 2009. His decision to retrace his steps back to engineering brought him to pursue a Master of Science degree at Louisiana State University. Oladapo has plans to pursue a Doctor of Philosophy in Chemical Engineering once he has obtained his masters.

Oladapo enjoys observing society, reading and playing soccer in his spare time.